AMERICAN SOCIETY FOR MICROBIOLOGY | Journal of Virology®

VIRUS-CELL INTERACTIONS

Folliculin Prevents Lysosomal Degradation of Human Papillomavirus To Support Infectious Cell Entry

Yoshiyuki Ishii,[a] Toshiyuki Yamaji,[b] Tsuyoshi Sekizuka,[a] Yuta Homma,[b] Seiichiro Mori,[a] Takamasa Takeuchi,[a] Iwao Kukimoto[a]

[a]Pathogen Genomics Center, National Institute of Infectious Diseases, Tokyo, Japan
[b]Department of Biochemistry and Cell Biology, National Institute of Infectious Diseases, Tokyo, Japan

ABSTRACT Human papillomavirus (HPV) infects epithelial basal cells in the mucosa and either proliferates with the differentiation of the basal cells or persists in them. Multiple host factors are required to support the HPV life cycle; however, the molecular mechanisms involved in cell entry are not yet fully understood. In this study, we performed a genome-wide clustered regularly interspaced short palindromic repeat (CRISPR)–CRISPR-associated protein 9 (Cas9) knockout (KO) screen in HeLa cells and identified folliculin (FLCN), a GTPase-activating protein for Rag GTPases, as an important host factor for HPV infection. The introduction of single guide RNAs for the *FLCN* gene into HeLa, HaCaT, and ectocervical Ect1 cells reduced infection by HPV18 pseudovirions (18PsVs) and 16PsVs. FLCN KO HeLa cells also exhibited strong resistance to infection with 18PsVs and 16PsVs; nevertheless, they remained highly susceptible to infections with vesicular stomatitis virus glycoprotein-pseudotyped lentivirus and adeno-associated virus. Immunofluorescence microscopy revealed that the numbers of virions binding to the cell surface were slightly increased in FLCN KO cells. However, virion internalization analysis showed that the internalized virions were rapidly degraded in FLCN KO cells. This degradation was blocked by treatment with the lysosome inhibitor bafilomycin A1. Furthermore, the virion degradation phenotype was also observed in Ras-related GTP-binding protein C (RagC) KO cells. These results suggest that FLCN prevents the lysosomal degradation of incoming HPV virions by enhancing lysosomal RagC activity.

IMPORTANCE Cell entry by human papillomavirus (HPV) involves a cellular retrograde transport pathway from the endosome to the *trans*-Golgi network/Golgi apparatus. However, the mechanism by which this viral trafficking is safeguarded is poorly understood. This is the first study showing that the GTPase-activating protein folliculin (FLCN) protects incoming HPV virions from lysosomal degradation and supports infectious cell entry by activating the Rag GTPases, presumably through the suppression of excessive lysosomal biosynthesis. These findings provide new insights into the effects of small GTPase activity regulation on HPV cell entry and enhance our understanding of the HPV degradation pathway.

KEYWORDS HPV, cell entry, FLCN, genome-wide CRISPR-Cas9 knockout screen

Human papillomaviruses (HPVs) infect epithelial basal cells in the skin or mucosa. Their proliferation is tightly associated with epithelial differentiation (1). Thus far, more than 200 genotypes of HPV have been identified (2). Among them, approximately 15 genotypes, including high-risk HPV16 and HPV18, are responsible for almost all cases of cervical cancer.

HPV is a nonenveloped virus composed of a circular double-stranded DNA genome (~8 kb) and the major/minor capsid proteins L1 and L2 (3). Because HPV propagates only in differentiating keratinocytes (4), preparations of authentic HPV virions generally yield only low numbers of viral particles. This impedes detailed studies on the

Editor Lawrence Banks, International Centre for Genetic Engineering and Biotechnology

Address correspondence to Yoshiyuki Ishii, yishii@nih.go.jp.
The authors declare no conflict of interest.

Received 12 January 2023
Accepted 20 April 2023
Published 11 May 2023

mechanism of infection of HPV. Hence, a surrogate virus was developed to investigate HPV infections. This virus is widely used and consists of a pseudovirion (PsV) that includes an HPV L1/L2 capsid encapsulating a reporter plasmid (5).

During the HPV life cycle, the virion initially binds to heparan sulfate (HS) proteoglycans on the cell surface or the basement membrane or to laminin-332 on the extracellular matrix (6–8). The binding of the virion to HS induces conformational changes in both the L1 and L2 capsid proteins (9–12). These changes facilitate the cleavage of these proteins by host proteases such as kallikrein-related peptidase 8 (KLK8) and furin (FURIN) (13, 14). These initial steps are crucial for virion uptake and the subsequent L2-mediated intracellular trafficking of virions. Over a long period of time, the virions enter the cells asynchronously by endocytosis that is possibly related to macropinocytosis in actin-dependent and clathrin-, caveolin-, cholesterol-, and dynamin-independent processes (15).

The penetration of L2 through the endosomal membranes occurs by γ-secretase coupled with p120-catenin (16–20). The protrusion of L2 allows the recruitment of the sorting nexin 17 (SNX17) protein (21), the retromer complex composed of vacuolar protein-sorting-associated protein 26 (Vps26)-Vps29-Vps35 (22), and the Rab7 GTPase-activating protein (GAP) TBC1 domain family member 5 (TBC1D5) (23) to L2. This recruitment is essential for the subsequent transport of the L2/viral genome (viral DNA [vDNA]) complex to the *trans*-Golgi network and the Golgi apparatus. Upon the G_2/M transition, the vesicles containing L2/vDNA are dispersed from Golgi stacks (24–27). Thereafter, the vesicles resulting from the protrusion of L2 through the endosomal membrane interact with a mitotic spindle motor protein complex containing Ran-binding protein 10 (RANBP10), karyopherin α2 (KPNA2), and dynein light chain Tctex type 3 (DYNLT3) (28). Finally, the L2/vDNA-containing vesicles bind to host mitotic chromosomes through the central chromosome-binding region of L2 (29).

The purpose of this study was to identify host factors required for HPV infection. Accordingly, we performed a genome-wide clustered regularly interspaced short palindromic repeat (CRISPR)–CRISPR-associated protein 9 (Cas9) knockout (KO) screen in HeLa cells infected with an HPV18 PsV (18PsV) containing an E2 expression plasmid. The screen produced a number of previously and newly reported cellular proteins that are associated with HPV infection. Among the latter proteins, we focused on the folliculin (FLCN) protein, whose mutations have been associated with Birt-Hogg-Dubé (BHD) syndrome, a genetic disorder characterized by fibrofolliculomas, renal tumors, lung cysts, and pneumothorax (30, 31).

FLCN is highly conserved across species and acts as a GAP for Ras-related GTP-binding protein C/D (RagC/D) (32). RagC/D regulates the mammalian target of rapamycin complex 1 (mTORC1) signaling cascade controlling the microphthalmia/transcription factor E (MiT/TFE) family, including transcription factor EB (TFEB) and transcription factor binding to IGHM enhancer 3 (TFE3) (32–34). Additionally, FLCN functions as a GAP for Rab7 GTPase, which mediates the lysosome-mediated degradation of epidermal growth factor receptor (EGFR) (35). Moreover, FLCN is a guanine nucleotide exchange factor for Rab35, thereby regulating EGFR intracellular trafficking (36, 37). Furthermore, it also acts as a Rab11A-interacting protein that is involved in the Rab11A-mediated recycling transport (38).

Here, by conducting a series of gene knockout experiments, we report that FLCN plays an important role in HPV infectious cell entry.

RESULTS

CRISPR-Cas9 KO screen in HeLa cells infected with HPV18 PsVs. We sought to identify genes required for HPV infection. For this purpose, we employed a negative-selection system using an HPV18 PsV containing an expression plasmid for the bovine papillomavirus E2 protein (18PsV-BE2); this system was originally described by Xie et al. (23). HeLa cells engineered to express the *Streptococcus pyogenes* Cas9 protein were transduced with a lentivirus (LV)-based single guide RNA (sgRNA) library for human

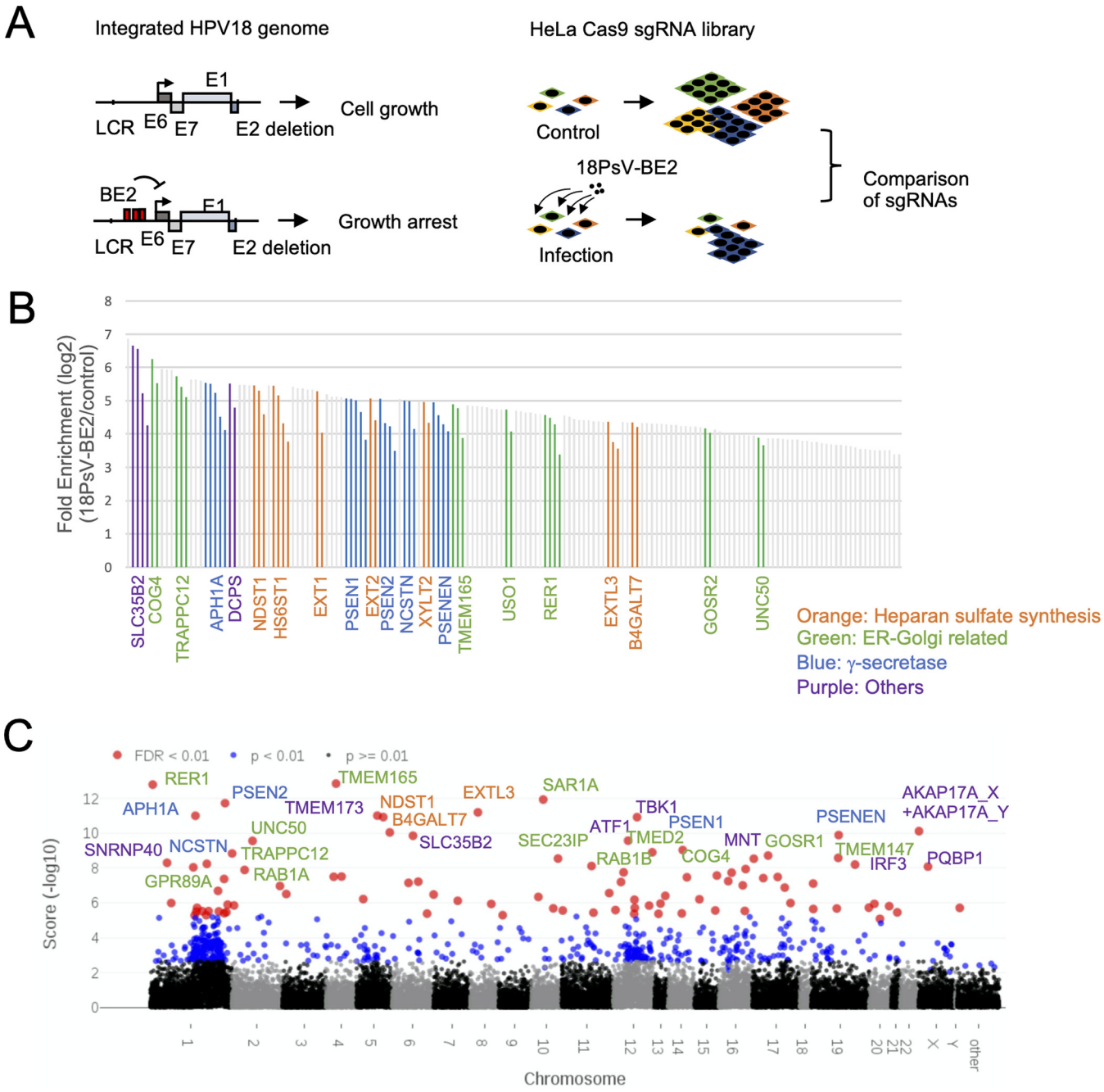

FIG 1 Genome-wide CRISPR-Cas9 screening to identify host genes required for HPV18 cell entry. (A, left) Effects of bovine papillomavirus E2 (BE2) on the growth of HeLa cells. (Right) Overview of the screen using the HPV18 pseudovirion containing the BE2 expression plasmid (18PsV-BE2). (B) Identification of sgRNAs enriched in the screen using HeLa cells. Fold enrichment shows sgRNAs enriched in two separate screenings and by >10-fold on average. Colored bars indicate that multiple sgRNAs were enriched, whereas gray bars indicate that a single sgRNA was enriched in a gene. The complete raw data sets are shown in Data Set S3 in the supplemental material. (C) Manhattan plot of the screen. Scores were derived from the MAGeCK analysis shown in Data Set S4. Red dots indicate a false discovery rate (FDR) of <0.01. Blue dots indicate a *P* value of <0.01 but an FDR of >0.01. Orange, green, blue, and purple labels show heparan sulfate synthesis, ER-Golgi-related, γ-secretase, and other genes, respectively.

genes. The resultant cells were infected with 18PsV-BE2. Once infection is established, E2 expressed from the PsV represses the transcription of E6/E7 from the viral promoter integrated into the HeLa genome and induces the arrest of cell growth (Fig. 1A, left) (39, 40). This process enables the enrichment of cells resistant to 18PsV-BE2 infection (i.e., cells with KO of genes essential for HPV infection) (Fig. 1A, right). A lentivirus-based genome-scale CRISPR-Cas9 KO (GeCKO) v2.0 pooled library was transduced into the Cas9-expressing HeLa cells. The library was delivered as two half-libraries (A and B)

TABLE 1 Gene ontology analysis of enriched sgRNA genes in the screen

Gene ontology term	*P* value ($-\log_{10}$)	Genes
Golgi transport complex	7.77E+00	COG8, COG7, COG6, COG5, COG4, COG3, COG2, COG1
Intra-Golgi vesicle-mediated transport	6.19E+00	RAB6C, COG8, COG6, COG5, GOSR2, GOSR1, COG3, COG2, COG1
trans-Golgi network membrane	5.56E+00	COG8, COG7, COG6, COG5, COG4, COG3, COG2, ARL1, COG1, TMEM165, VPS53, VAMP4, LGR5
Heparan sulfate proteoglycan biosynthetic process	5.26E+00	EXT1, NDST2, EXT2, NDST1, B3GAT3, XYLT2, EXTL3
Glycosaminoglycan biosynthetic process	4.63E+00	EXT1, NDST2, EXT2, NDST1, B3GAT3, XYLT2, HS6ST1, B4GALT7, EXTL3
Positive regulation of TOR signaling	1.14E+01	WDR59, MIOS, WDR24, FLCN, RRAGA, GOLPH3, RRAGC, MLST8, RICTOR, LAMTOR2, LAMTOR1, LAMTOR3, LAMTOR5
Ragulator complex	3.41E+00	LAMTOR2, LAMTOR1, LAMTOR3, LAMTOR5
Cornified envelope	3.61E+00	LCE3D, LCE3B, PRR9, SPRR2A, LCE1F, SPRR2B, LCE3E, LOR
Proteasome accessory complex	6.75E+00	PSMD6, PSMD12, PSMC5, PSMD11, PSMC6, PSMC3, PSMD13, PSMD3
Regulation of cellular amino acid metabolic process	4.00E+00	PSMD6, PSMD12, PSMC5, PSMD11, PSMC6, PSMC3, PSMD13, PSMD3, OAZ1
Proteasome complex	3.64E+00	USP14, PSMD6, PSMD12, PSMC5, PSMD11, PSMC6, PSMC3, PSMD13, PSMD3
Nuclear proteasome complex	2.98E+00	PSMD12, PSMC5, PSMC6, PSMC3
Proteasome regulatory particle, lid subcomplex	2.98E+00	PSMD12, PSMD11, PSMD13, PSMD3
Amyloid precursor protein catabolic process	4.35E+00	APH1A, PSENEN, NCSTN, PSEN2, PSEN1
Membrane protein ectodomain proteolysis	3.45E+00	APH1A, PSENEN, NCSTN, PSEN2, PSEN1, SPPL3

targeting a total of 19,050 human genes, with six sgRNAs per gene. Two independently prepared types of sgRNA-expressing HeLa cells (A-1, A-2, B-1, and B-2) were infected with 18PsV-BE2 and cultured for 2 weeks. High-throughput sequencing was used to determine the sequences of sgRNAs that had been integrated into the genomes of the surviving cells (see Data Sets S1 and S2 in the supplemental material).

Two independent screens revealed the enrichment of a total of 160 sgRNA sequences for 118 genes; among these, 21 genes containing multiple sgRNAs had been enriched by more than 10-fold on average (Fig. 1B and Data Set S3). The multiple sgRNAs included genes for the synthesis of HS (*NDST1*, *HS6ST1*, *EXT1*, *EXT2*, *XYLT2*, *EXTL3*, and *B4GALT7*), genes for the γ-secretase complex (*APH1A*, *PSEN1*, *PSEN2*, *NCSTN*, and *PSENEN*), and genes related to the endoplasmic reticulum (ER) and the Golgi apparatus (*COG4*, *TRAPPC12*, *TMEM165*, *USO1*, *RER1*, *GOSR2*, and *UNC50*). Model-based analysis of genome-wide CRISPR-Cas9 KO (MAGeCK) also showed high scores for genes required for the synthesis of HS, the γ-secretase complex, and the ER and Golgi apparatus (Fig. 1C and Data Set S4). Additionally, gene ontology analysis of the obtained data set revealed the enrichment of the "positive regulation of target of rapamycin (TOR) signaling," the "Ragulator complex," the "cornified envelope," and the "proteasome complex" (Table 1). Importantly, it was previously reported that HS and γ-secretase are essential for HPV infection (6, 7, 17, 18, 20, 41), thus demonstrating that this data set is suitable for analyzing the process of HPV infection.

Validation of the primary screen. Subsequently, we sought to validate the screening results. Therefore, sgRNAs for the candidate genes (Fig. 1B and C) were individually transduced into HeLa cells to assess the effects on HPV infection. HeLa cells were transfected with each sgRNA expression plasmid containing the Cas9 and puromycin resistance genes and were selected with puromycin. The surviving cells were inoculated with 18PsVs that contained a reporter plasmid expressing the firefly luciferase gene (18PsV-Luc) and cultured for an additional 48 h. Next, the reporter activity in infected cells was measured and normalized to the cell viability.

As shown in Fig. 2, the transfection of the sgRNA plasmids for genes required for the synthesis of HS (*NDST1*, *HS6ST1*, *EXT1*, *EXT2*, *XYLT2*, *EXTL3*, and *B4GALT7*); genes for the γ-secretase complex (*APH1A*, *PSEN1*, *PSEN2*, *NCSTN*, and *PSENEN*); TOR signaling-associated genes (*FLCN*, Ras-related GTP binding A [*RRAGA*], *RRAGC*, and rapamycin-insensitive companion of mTOR [*RICTOR*]); and genes related to the ER, the Golgi apparatus, and vesicle transport (*UNC50*, *RER1*, *TRAPPC12*, *COG4*, *TRAPPC13*, *SEC31A*, *SEC23IP*, *SEC23B*, G-protein-coupled receptor 89A [*GPR89A*], *GPR89B*, *RAB1A*, *RAB1B*, *TMEM147*, *USO1*, *TBC1D5*, and *GOSR2*) inhibited 18PsV-Luc infection by more than 20% compared with the control cells. Moreover, the introduction of sgRNAs for proteasome 26S subunit non-ATPase 12 (*PSMD12*), ubiquitin-protein ligase E3D (*UBE3D*), *FURIN*, PDS5 cohesin-associated factor A

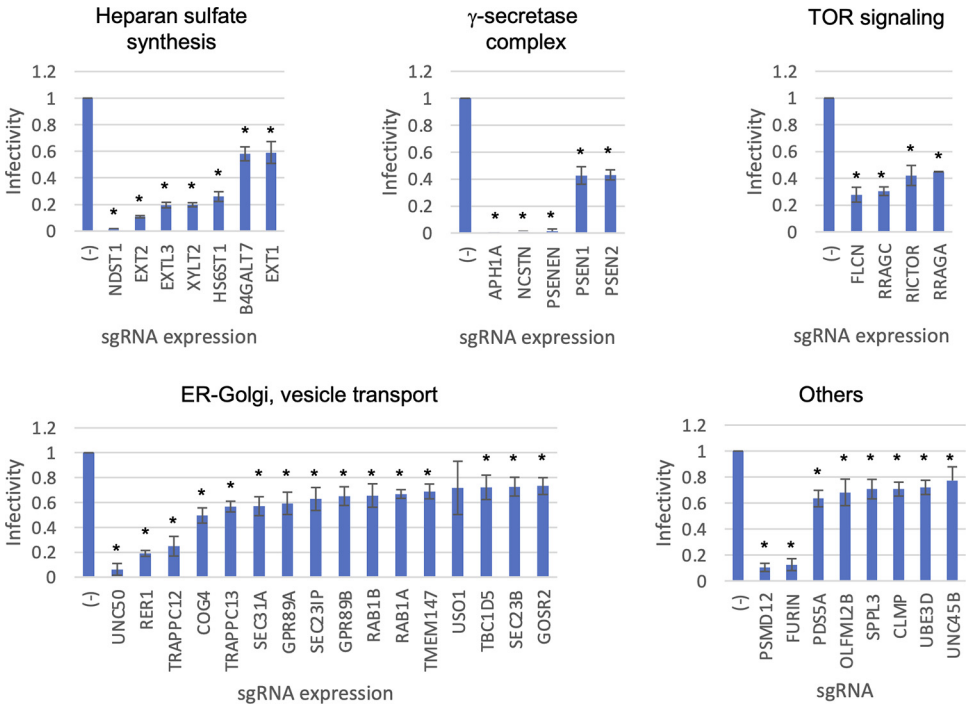

FIG 2 Infection with HPV18 pseudovirions (18PsVs) in HeLa cells expressing sgRNAs for individual candidate genes. Each sgRNA was transduced into HeLa cells. Untransfected cells were excluded by puromycin selection, while successfully transfected cells were subsequently infected with 18PsVs containing the luciferase reporter plasmid (18PsV-Luc). At 48 h postinfection (hpi), the luciferase activity in the cells was measured and normalized to the cell viability. Data are shown as the means ± standard deviations from three independent experiments. (−), empty plasmid. Statistical analysis was performed using Student's *t* test. *, $P < 0.05$.

(*PDS5A*), olfactomedin-like protein 2B (*OLFML2B*), signal peptide peptidase-like 3 (*SPPL3*), CXADR-like membrane protein (*CLMP*), and unc-45 myosin chaperone B (*UNC45B*) also significantly decreased the levels of infection. These results further verified the integrity of our CRISPR-Cas9 KO screen.

FLCN is required for effective HPV infection. Among the genes identified by screening, we focused on *FLCN*, which encodes the intracellular GAP FLCN, because the involvement of this gene in the HPV life cycle has not yet been reported. Initially, in addition to the sgRNA in Fig. 2 (FLCN-1), we used another sgRNA for *FLCN* (FLCN-2) to confirm the effects of FLCN KO on HPV infection. Western blot analysis confirmed that FLCN expression was almost completely diminished in HeLa cells transfected with these sgRNAs (Fig. 3A, bottom). Under these conditions, infection by 18PsV-Luc and 16PsV-Luc was significantly suppressed compared with that observed in control cells (Fig. 3A). FLCN KO was also examined for two other cell lines, namely, immortalized human keratinocyte HaCaT cells and HPV16 E6/E7-expressing ectocervical Ect1/E6E7 cells. Following FLCN KO, both types of cells also exhibited significant reductions in PsV infection (Fig. 3B).

Next, we generated FLCN KO HeLa cells by transient transfection with the CRISPR-Cas9 plasmid and examined their susceptibility to PsV infection. Sequence analysis of the genomic DNA from an FLCN KO clone (ΔFLCN) demonstrated that the coding sequences in exon 3 of *FLCN* were frameshifted in both alleles. Western blot analysis confirmed that FLCN expression was completely abolished in the ΔFLCN cells (Fig. 3C). In infection assays, these cells were approximately 80% less susceptible to each PsV infection than the parental cells (Fig. 3D). Importantly, the reintroduction of wild-type FLCN cDNA fused with a hemagglutinin (HA) tag at the C terminus into ΔFLCN cells (ΔFLCN/FLCN-HA) restored the levels of PsV infection even beyond those noted for the parental cells (Fig. 3D). This observation confirmed that the reduction of HPV infection was caused by the loss of FLCN expression.

We also tested whether infection by other viruses was also affected by FLCN KO.

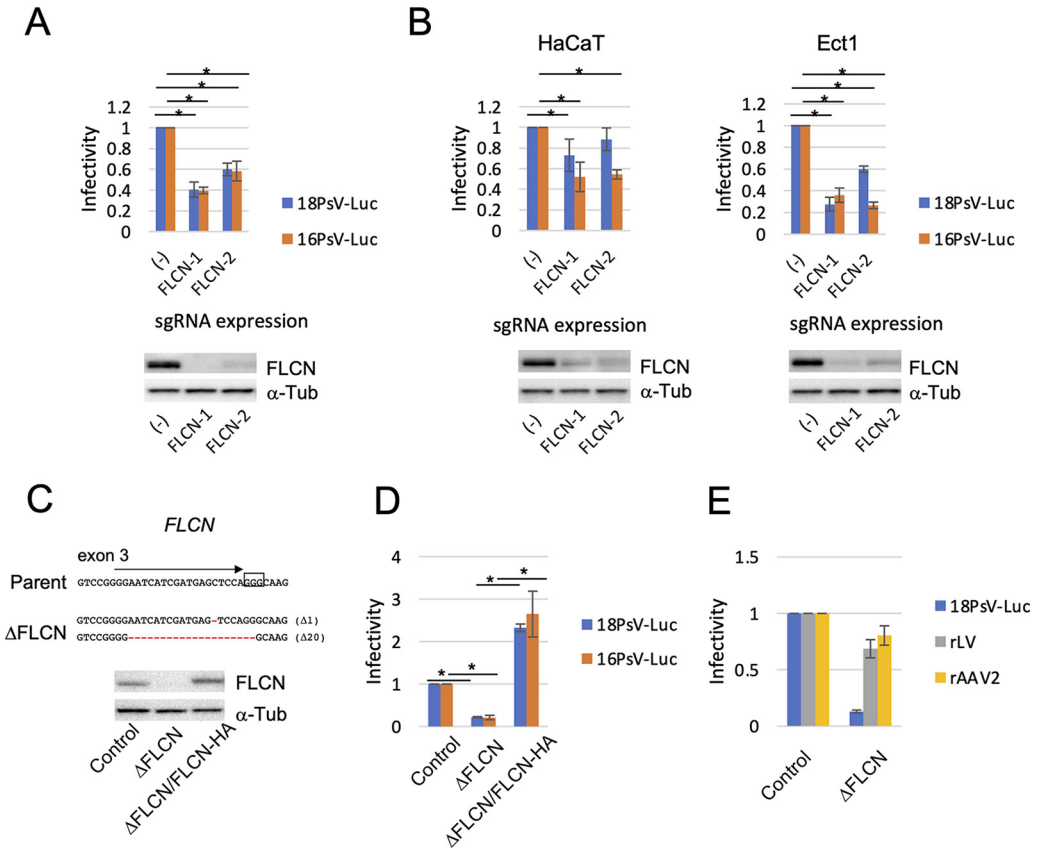

FIG 3 Effects of FLCN depletion on PsV infection. (A) Infectivity of 18PsV-Luc and HPV16 PsVs containing the luciferase expression plasmid (16PsV-Luc) in HeLa cells transfected with different FLCN sgRNA expression plasmids (FLCN-1 and FLCN-2) or an empty vector (−). The bottom panels show Western blotting of cell lysates stained with anti-FLCN and labeled anti-α-tubulin (α-Tub) antibodies, respectively. (B) Infectivity of PsVs in HaCaT and Ect1 cells transduced with FLCN sgRNA-expressing lentiviruses. The bottom panels represent Western blotting of the transduced cells. (C) Construction of FLCN KO and FLCN-reintroduced HeLa cells. (Top) The FLCN KO exon 3 sequence, in which red hyphens indicate deleted nucleotides causing frameshift mutations (ΔFLCN). The box indicates the protospacer-adjacent motif (PAM) sequence. (Bottom) Western blotting of the lysates of parental (control), ΔFLCN, and FLCN-reintroduced ΔFLCN (ΔFLCN/FLCN-HA) cells. (D) Infectivity of PsVs in control, ΔFLCN, and ΔFLCN/FLCN-HA cells. (E) Infectivity of lentivirus pseudotyped with vesicular stomatitis virus glycoprotein (rLV) and recombinant adeno-associated virus serotype 2 (rAAV2) in control and ΔFLCN HeLa cells. All data in the graphs are shown as the means ± standard deviations from three independent experiments. Statistical analysis was performed using Student's *t* test. *, $P < 0.05$.

For this purpose, we infected the ΔFLCN cells with a recombinant lentivirus pseudotyped with the glycoprotein of vesicular stomatitis virus (rLV) or recombinant adeno-associated virus (AAV) serotype 2 (rAAV2). As shown in Fig. 3E, following FLCN KO, the cells were highly susceptible to infection with rLV or rAAV2. These findings showed that FLCN KO did not block lentiviral or AAV transduction, suggesting that the loss of FLCN does not cause broad defects in cellular physiology supportive of general endocytosis or viral transduction.

FLCN protects incoming HPV virions from lysosomal degradation. Using immunofluorescence microscopy, we examined virion binding to the cell surface to investigate the mechanism by which HPV infection was blocked in FLCN KO cells. The ΔFLCN, ΔFLCN/FLCN-HA, and parental cells were incubated with 18PsV-Luc at 4°C for 1 h and fixed with paraformaldehyde. The cell surfaces were subsequently immunolabeled with monoclonal anti-HPV18 L1 antibodies and observed by confocal fluorescence microscopy. As shown in Fig. 4A and B, the fluorescence signals on the cell surfaces of ΔFLCN cells were approximately 1.5-fold higher than those of the control and ΔFLCN/FLCN-HA cells. After immunolabeling with anti-HS antibodies, the expression levels of HS were also higher in ΔFLCN cells than in the control and ΔFLCN/FLCN-HA cells. In contrast, β-1,3-glucuronyltransferase 3 (B3GAT3) KO cells with HS deleted (Fig. 4C)

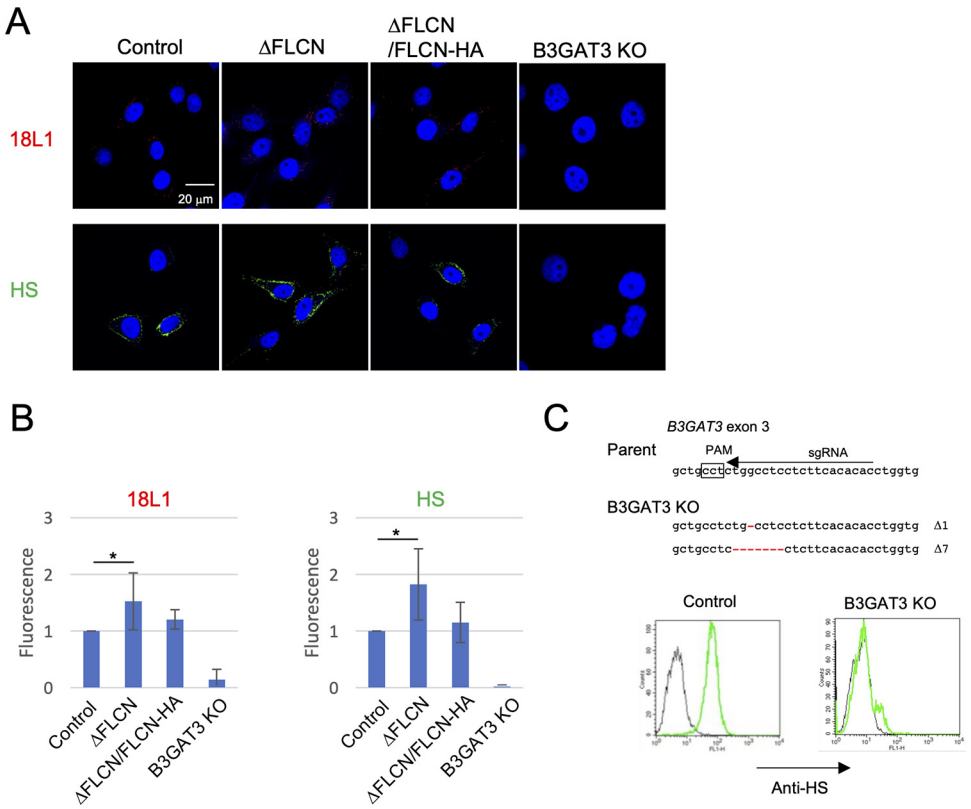

FIG 4 PsV binding to the cell surface of FLCN knockout (KO) cells. (A) Parental (control), ΔFLCN, ΔFLCN/FLCN-HA, and B3GAT3 KO (depleted of heparan sulfate [HS] and chondroitin sulfate) cells were incubated with 18PsV-Luc at 4°C for 1 h and fixed with paraformaldehyde. The cells were incubated with HPV18 L1 capsid (18L1) antibody or HS antibody, followed by incubation with secondary antibodies. The cells were visualized by confocal immunofluorescence microscopy. 18L1 and HS are shown as red and green signals, respectively. B3GAT3 KO cells were used as negative controls. (B) Quantification of virions binding to the cell surface. The fluorescence in four different fields (approximately 10 cells per field) was measured using FluoView FV1000 software and averaged. All data in the graphs are shown as the means ± standard deviations from three independent experiments. Statistical analysis was performed using Student's *t* test. *, $P < 0.05$. (C) Generation of B3GAT3 KO HeLa cells. (Top) The exon 3 sequence of B3GAT3, in which red hyphens indicate deleted nucleotides causing frameshift mutations. The box indicates the protospacer-adjacent motif (PAM) sequence. (Bottom) Fluorescence-activated cell sorting analysis using the anti-HS antibody.

showed negligible levels of binding to 18PsV-Luc, indicating the requirement of HS for PsV cell binding. These results suggest that FLCN KO increases the expression of HS, leading to the slightly enhanced binding of the virion to the cell.

Next, we investigated the subcellular localization of virions using 18PsVs and 16PsVs that were labeled with 5-ethynyl-2′-deoxyuridine (EdU), which enables the visualization of the reporter plasmid through the Click-iT reaction. The ΔFLCN, ΔFLCN/FLCN-HA, and parental cells were incubated with the EdU-labeled PsVs (18PsV-EdU or 16PsV-EdU) at 37°C for 2 or 8 h; fixed; permeabilized; and examined using the Click-iT reaction. The subcellular localization of early endosome antigen 1 (EEA1) (an early endosome marker) was also visualized with anti-EEA1 antibodies. As shown in Fig. 5A, the colocalization of the EdU-labeled PsVs and EEA1-associated endosomes was significantly reduced in the ΔFLCN cells compared with the control cells after both 2- and 8-h incubations; this defect was restored in the ΔFLCN/FLCN-HA cells. The overlapping signal between EEA1 and EdU staining was quantified and statistically evaluated using Pearson's correlation coefficient (Fig. 5A, right). Next, GM130 (a *cis*-Golgi marker) was visualized using anti-GM130 antibodies to examine the Golgi localization of the virion (Fig. 5B). After incubation for 2 h, PsVs were not colocalized with GM130 in any of the cell types except ΔFLCN/FLCN-HA cells with 18PsVs (Fig. 5B, right). Following incubation for 8 h, the colocalization of PsVs and GM130 was significantly increased in control cells versus ΔFLCN cells, and the colocalization was restored in ΔFLCN/

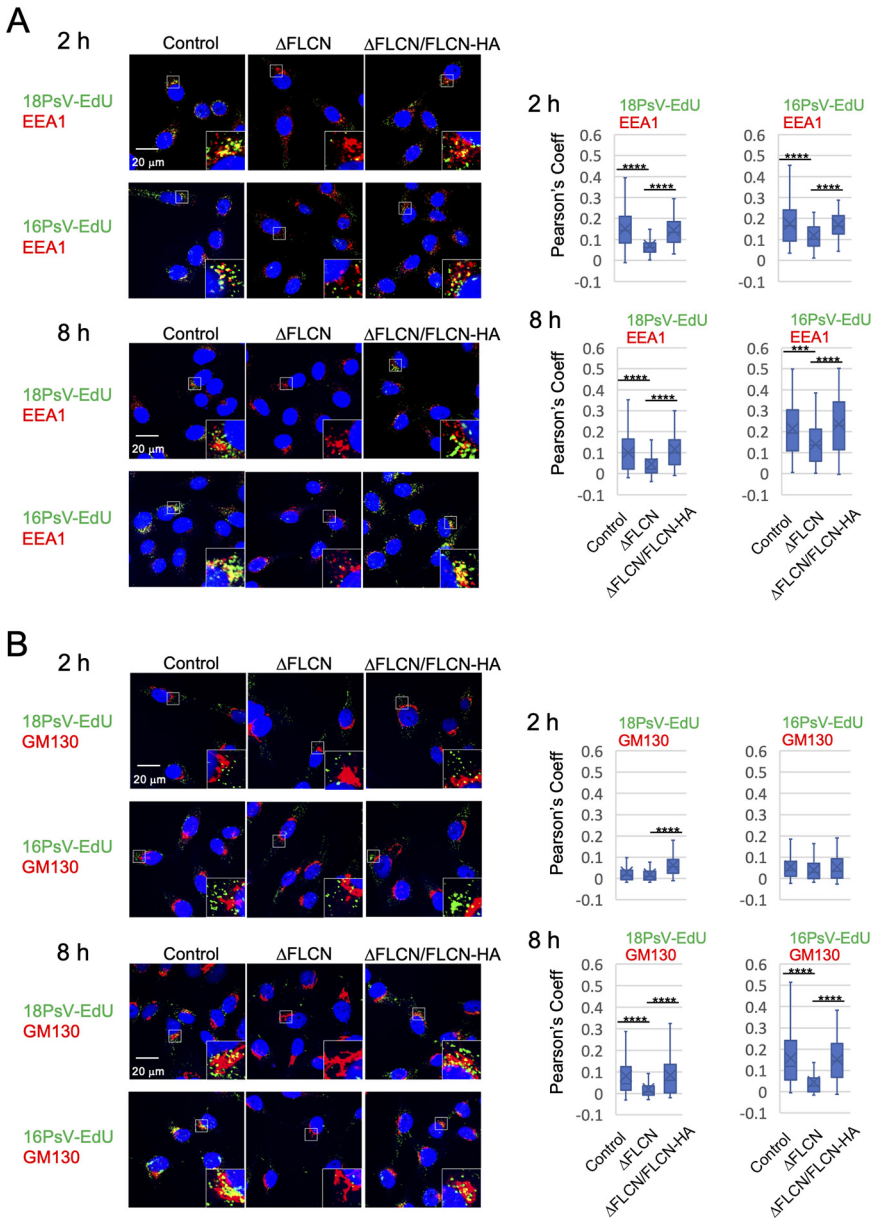

FIG 5 Subcellular localization of PsVs in FLCN knockout cells. (Left panels) Control, ΔFLCN, and ΔFLCN/FLCN-HA cells were incubated with EdU-labeled 18PsV-Luc (18PsV-EdU) or 16PsV-Luc (16PsV-EdU) at 37°C for 2 or 8 h. EdU was detected using the Click-iT reaction. EEA1, an early endosome marker (A), and GM130, a *cis*-Golgi marker (B), were stained with specific antibodies. EdU and antibodies were visualized by confocal immunofluorescence microscopy. EdU staining is shown as a green signal. EEA1 and GM130 staining is shown as a red signal. The boxed area is enlarged in the bottom right corner. (Right panels) The colocalization signals in the merged images from at least 30 cells were quantified using FluoView FV1000 software, and the Pearson correlation coefficient (Coeff) was determined. Each bar represents the minimum (25th percentile), median (75th percentile), and maximum values. Crosses represent mean values. ***, $P < 0.005$; ****, $P < 0.001$ (by Student's *t* test).

FLCN-HA cells. Although the reduced fluorescence of EdU-labeled pseudoviral DNA in the FLCN KO cells is not an optimal condition to study the colocalization of PsVs and organelle markers, it nevertheless suggests that PsV uptake is inhibited or PsV degradation is induced in FLCN KO cells.

We thus examined whether FLCN KO affected virion uptake. The ΔFLCN, ΔFLCN/FLCN-HA, and parental cells were incubated with 16PsV-Luc at 4°C for 1 h. After the removal of unbound virions, the cells were cultured at 37°C for 0, 1, 2, 4, and 8 h. Next, the cells were detached using EDTA with or without trypsin. HPV16 L1 (16L1) extracted

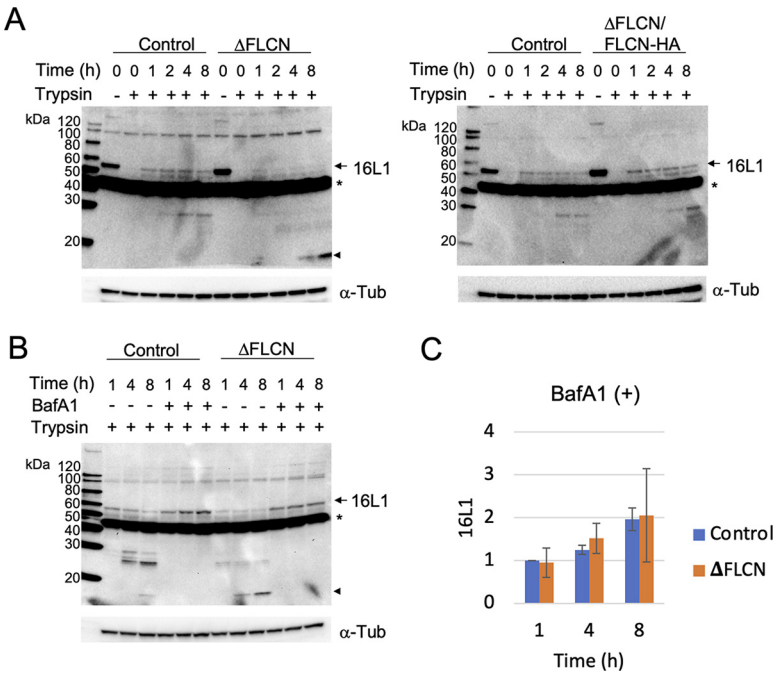

FIG 6 Internalization of 16PsV-Luc in FLCN (folliculin) knockout cells. (A) Control, ΔFLCN (FLCN KO clone), and ΔFLCN/FLCN-HA cells, which were incubated with 16PsV-Luc at 4°C for 1 h, were detached from culture dishes using EDTA (time zero, Trypsin −) or trypsin-EDTA (time zero, Trypsin +) or incubated with growth medium at 37°C for the indicated times and subsequently detached using trypsin-EDTA. 16PsV-Luc in detached cells was analyzed by Western blotting using the anti-HPV16 (human papillomavirus 16) L1 antibody. The arrows and the arrowhead show full-length L1 proteins (16L1) and bands of approximately 15 kDa, respectively. 16PsV, HPV16 pseudovirion; HA, hemagglutinin; Luc, luciferase; *, unknown nonspecific cellular protein. (B) Control and ΔFLCN cells, which had been incubated with 16PsV-Luc at 4°C for 1 h, were cultured in medium with (+) or without (−) bafilomycin A1 (BafA1) at 37°C. Thereafter, the cells were detached from the plates using trypsin-EDTA and analyzed by Western blotting with the anti-16L1 antibody. (C) Quantification of 16L1 in control and ΔFLCN cells after incubation for 8 h in the presence of BafA1. The intensity of the 16L1 bands was quantified using the ChemiDoc XRS+ system. All data were normalized to the levels of α-tubulin (α-Tub) and are shown as the means ± standard deviations from three independent experiments. Statistical analysis was performed using Student's *t* test.

from the cell lysates was analyzed by Western blotting with anti-HPV16 L1 antibodies. At the start of the incubation (0 h), L1 was not detected in the lysates of trypsin-treated cells, indicating that the virions had not yet been incorporated into the cells (Fig. 6A). Following incubation for 1 h, trypsin-resistant, intact L1 was detectable in the parental and ΔFLCN/FLCN-HA cells, which indicated virion internalization. In contrast, trypsin-resistant L1 was barely detectable in the ΔFLCN cells throughout the incubation. Notably, a short fragment of L1 (~15 kDa) (Fig. 6A, arrowhead) became detectable after incubation for 4 and 8 h. This finding suggests that FLCN KO may promote the proteolytic degradation of incoming HPV virions rather than inhibiting the internalization of virions. To examine this hypothesis, the cells were incubated with 16PsVs for 8 h in a medium containing bafilomycin A1 (a V-ATPase inhibitor that blocks lysosomal degradation) and detached using trypsin-EDTA. As shown in Fig. 6B, the short L1 fragment was no longer detected in the presence of bafilomycin A1; in contrast, the intact, trypsin-resistant L1 fragment appeared in place of the short L1 fragment. Quantification of the band intensity of full-length L1 did not reveal a significant difference between the control and ΔFLCN cells in the presence of bafilomycin A1 (Fig. 6C). Collectively, these results indicate that the internalization of HPV virions is not impaired in FLCN KO cells; however, the internalized virions are rapidly directed toward degradation in the lysosome.

Effects of FLCN knockout on the degradation of cellular proteins. To determine whether other cellular proteins were also degraded in the FLCN KO cells, we monitored the uptake of transferrin (Tf), which is transported via the early/late endosomes and

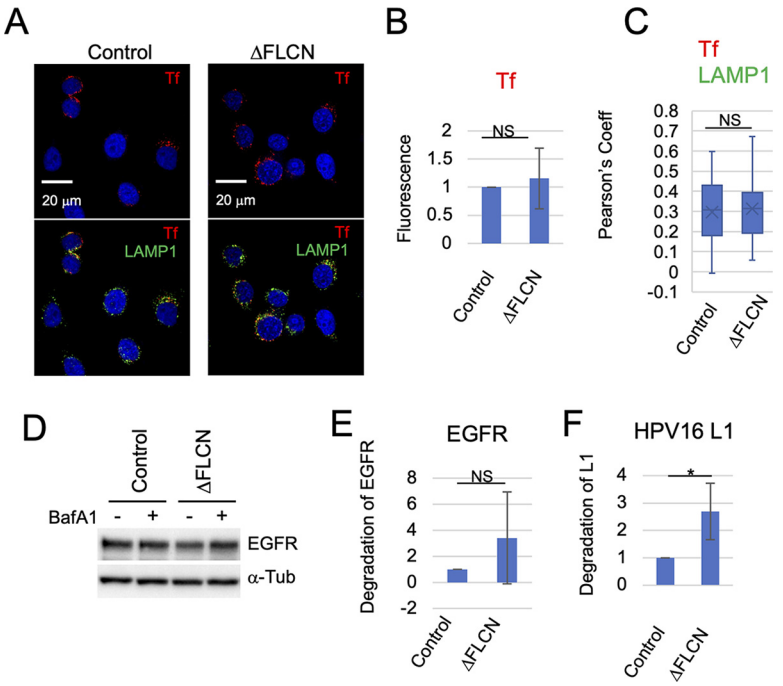

FIG 7 Internalization of transferrin (Tf) and epidermal growth factor receptor (EGFR) in FLCN knockout cells. (A) Microscopic images of the endocytotic uptake of Tf. HeLa mCAT8 (control) or ΔFLCN cells were incubated with Tf conjugated with Alexa Fluor 568 at 4°C for 1 h and cultured at 37°C for 15 min. After cell surface-bound Tf was removed by treatment with DMEM containing 25 mM sodium acetate (pH 2.0), the cells were incubated with rabbit anti-LAMP1 antibody and anti-rabbit IgG conjugated with Alexa Fluor 488. (B) The fluorescence in three different fields (approximately 10 cells per field) was quantified using FluoView FV1000 software and averaged. The data are shown as the means ± standard deviations from three independent experiments. Statistical analysis was performed using Student's *t* test. (C) The colocalization signals between Tf and LAMP1 in the merged images obtained from at least 30 cells were quantified using FluoView FV1000 software, and Pearson's correlation coefficient was calculated. Each bar represents the minimum (25th percentile), median (75th percentile), and maximum values. Crosses represent mean values. NS, not statistically significant (by Student's *t* test). (D) Western blot analysis of EGFR. HeLa mCAT8 (control) or ΔFLCN cells were cultured with (+) or without (−) bafilomycin A1 (BafA1) at 37°C for 1 h. The cells were detached from the plates with trypsin-EDTA, and the cell extracts were analyzed by Western blotting with anti-EGFR antibody. The top and bottom panels indicate intact EGFR and α-tubulin, respectively. (E) Quantification of the levels of degradation of EGFR in control and ΔFLCN cells. The band intensity of EGFR was quantified using the ChemiDoc XRS+ system and normalized to that of α-tubulin. Degradation levels were quantified from the band intensity of EGFR with BafA1 versus that of EGFR without BafA1. The data are shown as the means ± standard deviations from three independent experiments. Statistical analysis was performed using Student's *t* test. (F) Quantification of the levels of degradation of full-length HPV16 L1 in cells treated with or without BafA1 as described above. The data are shown as the means ± standard deviations from three independent experiments. *, $P < 0.05$; NS, not statistically significant (by Student's *t* test).

lysosome for degradation (42), by fluorescence microscopy analysis (Fig. 7A). The fluorescence level of Tf (Fig. 7B) and its colocalization with lysosome-associated membrane protein 1 (LAMP1) (a late endosome/lysosome marker) (Fig. 7C) were not significantly different between the control and FLCN KO cells, suggesting that FLCN KO does not affect the degradation of Tf. In addition, we analyzed the cellular levels of EGFR, also known to be transported via the early/late endosomes and lysosome for degradation (43), by Western blot analysis. As shown in Fig. 7D, the EGFR levels were slightly elevated in the presence of bafilomycin A1 in both the control and FLCN KO cells, indicating its normal lysosomal degradation. Quantification of the band intensity revealed that the level of degradation was approximately 3-fold higher in the FLCN KO cells than in the control cells but did not reach statistical significance (Fig. 7E). In contrast, L1 degradation was significantly increased in the FLCN KO cells under the same experimental conditions (Fig. 7F). These results suggests that increased degradation by FLCN KO is not common to other cellular cargos but rather is specific to HPV virions.

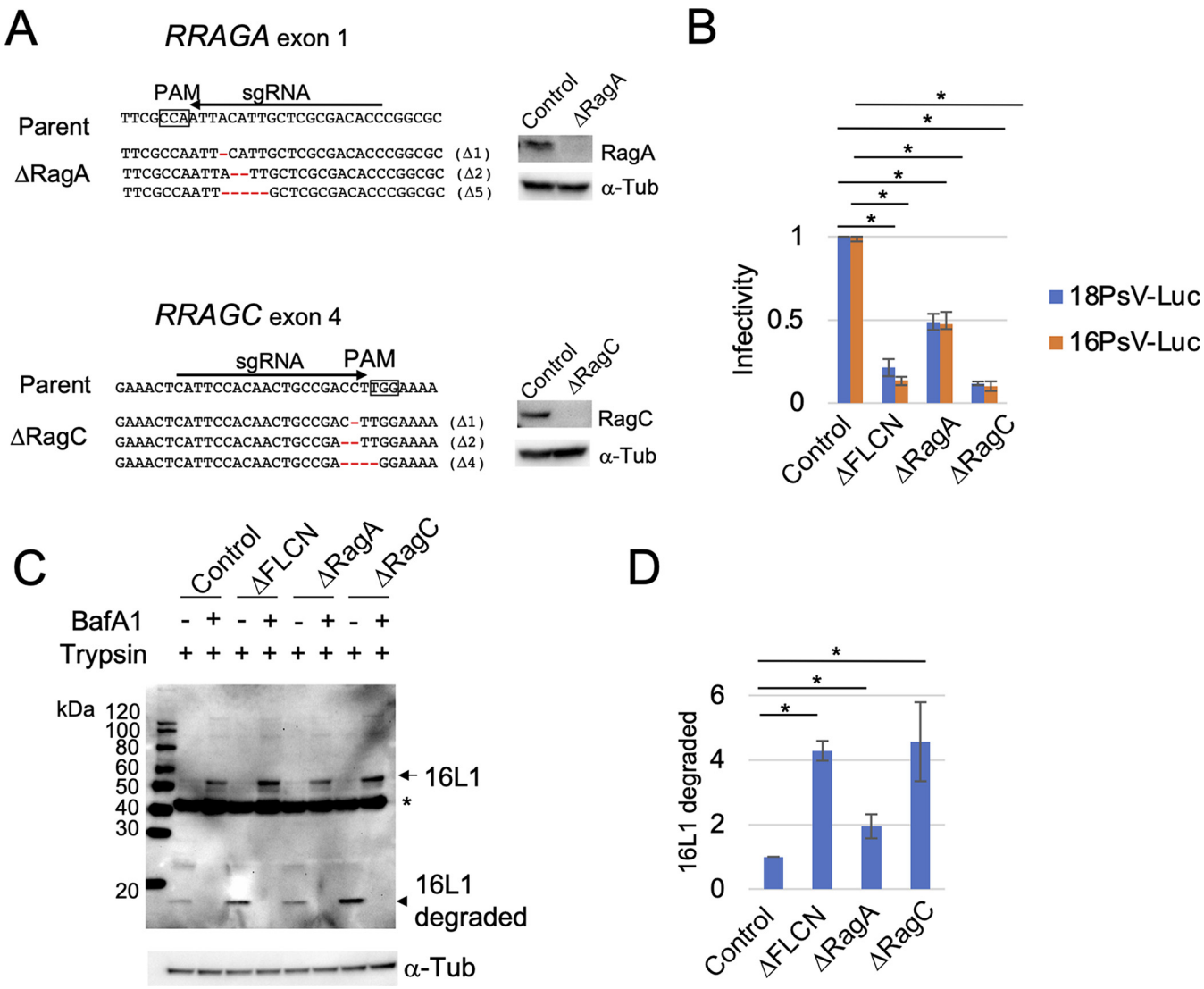

FIG 8 Effects of RagA and RagC knockout (KO) on 16PsV-Luc infection. (A) Construction of small GTPase RagA KO and RagC KO HeLa cells. (Left) The *RRAGA* KO exon 1 sequence and the *RRAGC* KO exon 4 sequence, in which red hyphens indicate deleted nucleotides causing frameshift mutations (ΔRagA and ΔRagC, respectively). The box indicates the protospacer-adjacent motif (PAM) sequence. (Right) Western blotting of the lysates of parental (control), ΔRagA, and ΔRagC cells. (B) Infection by PsVs in control, ΔFLCN, ΔRagA, and ΔRagC cells. (C) Control, ΔFLCN, ΔRagA, and ΔRagC cells, which were incubated with 16PsV-Luc at 4°C for 1 h, were cultured in medium with (+) or without (−) bafilomycin A1 (BafA1) at 37°C for 8 h. The cells were detached from the plates using trypsin-EDTA and analyzed by Western blotting with the anti-16L1 antibody. (D) Quantification of 16L1 degradation after incubation for 8 h in the absence of BafA1. The band intensity of the ~15-kDa 16L1 fragment (16L1 degraded) was quantified using the ChemiDoc XRS+ system. All data were normalized to the levels of α-tubulin and are shown as the means ± standard deviations from three independent experiments. Statistical analysis was performed using Student's *t* test. *, $P < 0.05$.

Phenotype of RagC KO cells for HPV infection. The Rag GTPase heterodimeric complexes are composed of RagA or RagB (RagA/B) with RagC or RagD (RagC/D) (44). Since FLCN functions as a GAP for RagC/D (32), and the knockout of RagC inhibited 18PsV infection as efficiently as the knockout of FLCN (Fig. 2), we examined whether RagC KO resulted in a phenotype for PsV infection similar to that of FLCN KO. To this end, HeLa cells with RagA or RagC KO were generated by CRISPR-Cas9 gene editing. As shown in Fig. 8A, genomic DNA from RagA KO (ΔRagA) and RagC KO (ΔRagC) cell clones revealed frameshifted deletions in the coding sequences in exon 1 of *RRAGA* and exon 4 of *RRAGC*. Western blot analysis confirmed the complete loss of RagA and RagC expression in ΔRagA and ΔRagC cells, respectively. In infection assays, both types of Rag KO cells showed reduced infection with each PsV versus the parental cells (~50% and ~80% reductions in ΔRagA and ΔRagC cells, respectively) (Fig. 8B). Of note, the level of reduction in ΔRagC cells was comparable

to that observed in ΔFLCN cells. We further examined whether Rag KO induced the lysosomal degradation of incorporated HPV virions in a manner similar to that of FLCN KO. The KO and control cells were incubated with 16PsVs for 8 h in the presence or absence of bafilomycin A1. Subsequently, the cells were detached with trypsin-EDTA and subjected to Western blotting. As shown in Fig. 8C, the short L1 fragment was easily detectable in ΔRagC cells (as in ΔFLCN cells), and its appearance was also completely blocked by treatment with bafilomycin A1. The band intensity of the short L1 fragment in ΔRagC cells was comparable to that observed in ΔFLCN cells (Fig. 8D). These results strongly suggest that RagC activity regulated by FLCN contributes to the lysosomal degradation of incoming HPV virions.

Intracellular localization of HPV virions in cells treated with lysosomal inhibitors. To further confirm the lysosomal degradation of PsVs by FLCN KO, we tested the effects of conventional lysosome protease inhibitors, E64d (a cysteine protease inhibitor) and pepstatin A (an aspartic protease inhibitor), on PsV trafficking. The ΔFLCN and parental cells were incubated with 16PsV-EdU in the presence or absence of a mixture of E64d-pepstatin A at 37°C for 8 h, followed by immunofluorescence analysis of EdU, 16L1, and RagC (a lysosome marker). As shown in Fig. 9A, in the absence of the inhibitors, weak fluorescence signals of EdU/16L1 and RagC colocalization were detected in the control cells, but such signals were hardly detectable in the FLCN KO cells. In the presence of the inhibitors, however, the level of EdU/16L1 and RagC colocalization was significantly increased in the control cells, and the same level of colocalization in the FLCN KO cells as that in the control cells was also observed (Fig. 9B). Western blot analysis of incorporated L1 proteins showed that the short L1 fragment was not detected in the FLCN KO cells treated with the lysosome protease inhibitors (Fig. 9C), as in the cells treated with bafilomycin A1. Overall, these results indicate that PsVs undergo lysosomal degradation in FLCN KO cells.

Effects of PsV infection on FLCN subcellular localization. Finally, we examined whether HPV infection alters the subcellular localization of FLCN to suppress virion degradation. ΔFLCN/FLCN-HA cells were incubated with (+) or without (−) 16PsV-EdU at 37°C for 2 h, followed by fluorescence labeling of EdU by the Click-iT reaction. FLCN-HA, EEA1, LAMP1, RagC, and mTOR were then visualized with their specific antibodies. As shown in Fig. 10, FLCN-HA was distributed in both the nucleus and the cytoplasm, and 16PsV-EdU infection did not induce the colocalization of FLCN-HA with EdU-labeled pseudoviral DNA or these organelle markers, suggesting that HPV infection does not affect the distribution or activation of FLCN and is thought to follow the authentic degradation pathway controlled by FLCN.

DISCUSSION

In this study, we performed genome-wide CRISPR-Cas9 KO library screening to explore the cellular proteins required for infection with HPV18 PsVs. This screening led to the discovery of several host proteins, both known and unknown, that are essential for successful HPV infection. Among these proteins, we focused on FLCN for further analysis. The results showed that FLCN KO significantly inhibited infection with 18PsVs or 16PsVs in cervical cancer cells as well as immortalized human keratinocytes and ectocervical cells transformed by the HPV16 oncogenes. FLCN KO cells showed strong resistance to infections with 18PsVs and 16PsVs; nevertheless, they remained highly susceptible to infections with rLV and rAAV2. Finally, FLCN KO induced the rapid degradation of internalized 16PsVs in the lysosome, indicating that FLCN is involved in preventing the lysosomal degradation of the HPV virion.

FLCN is a GAP that induces the activation of the small GTPase RagC/D on the lysosomal membrane (32). Thus, the degradation of HPV virions observed in FLCN KO cells implies that RagC/D activity controls the lysosomal degradation of incoming virions. Indeed, RagC KO cells exhibited phenotypes similar to those of FLCN KO cells for PsV cell entry and degradation. The MiT/TFE transcription factors are phosphorylated and inactivated by mTORC1 that is recruited to the lysosome by the active, GDP-bound form of RagC/D in response to amino acid stimulation (45), thereby leading to the suppression

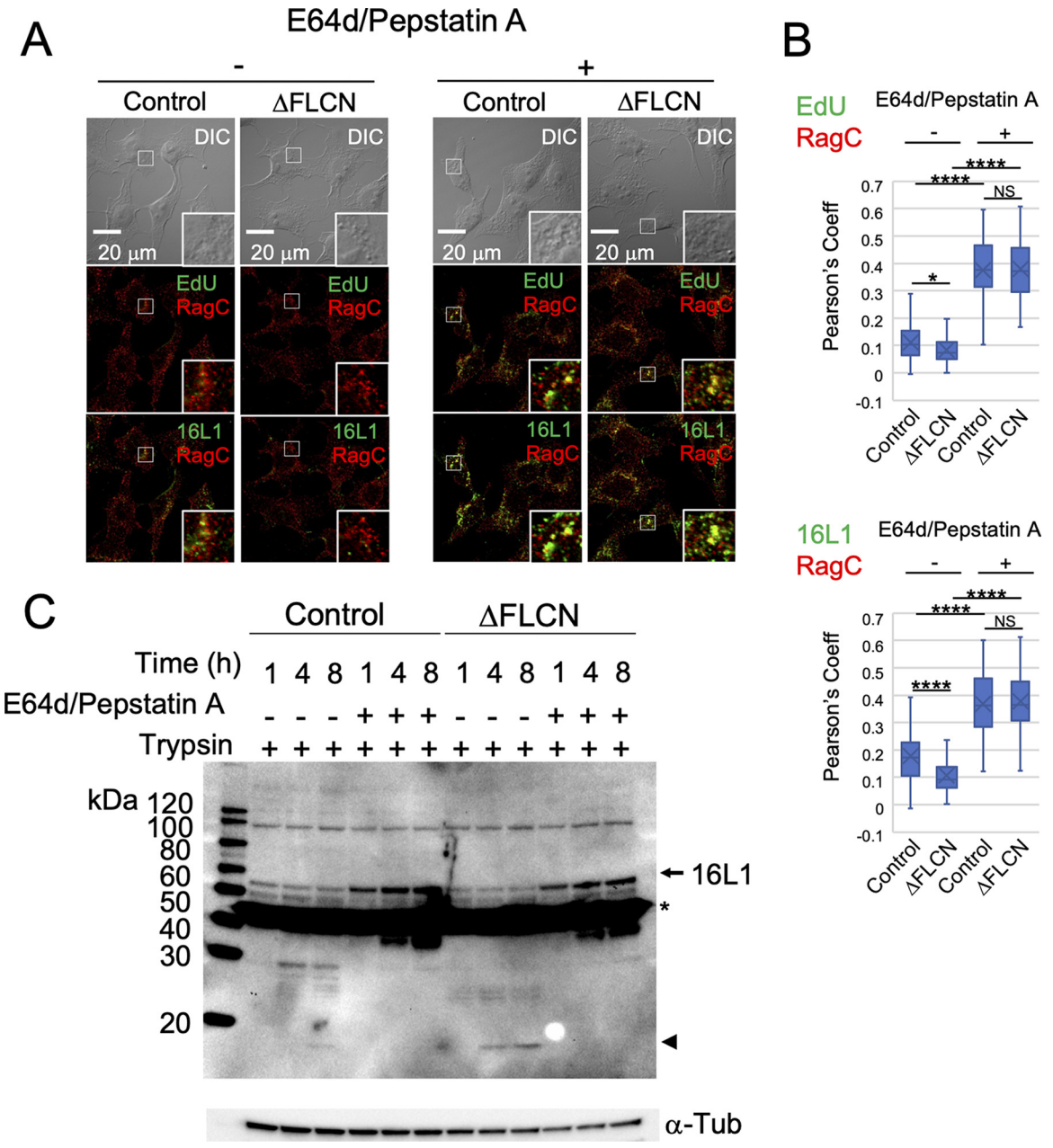

FIG 9 Intracellular localization of HPV virions in cells treated with lysosomal inhibitors. (A) Subcellular localization of 16PsVs in the presence of lysosome protease inhibitors. Control and ΔFLCN cells were incubated with 16PsV-EdU in the presence (+) or absence (−) of 87.6 μM E64d and 43.7 μM pepstatin A (E64d/Pepstatin A) at 37°C for 8 h. EdU and HPV16 L1 (16L1) were detected using the Click-iT reaction and mouse anti-33L1-7 antibody, respectively. RagC (a lysosome marker) was stained with rabbit anti-RagC (clone D8H5, catalog number 9480; Cell Signaling Technology). The fluorescence of EdU and antibodies was visualized by confocal microscopy. EdU and 16L1 staining is shown as a green signal. RagC staining is shown as a red signal. The boxed area is enlarged in the bottom right corner. DIC, differential interference contrast. (B) The colocalization signals in the merged images from at least 30 cells were quantified using FluoView FV1000 software, and Pearson's correlation coefficient was determined. Each bar represents the minimum (25th percentile), median (75th percentile), and maximum values. Crosses represent mean values. *, $P < 0.05$; ****, $P < 0.001$; NS, not statistically significant (by Student's t test). (C) Internalization of 16PsVs in the presence of E64d and pepstatin A. Control and ΔFLCN cells, which had been incubated with 16PsVs for 1 h at 4°C, were cultured in medium with (+) or without (−) E64d/Pepstatin A at 37°C. The cells were detached from the plates using trypsin-EDTA and analyzed by Western blotting with the anti-16L1 antibody. The arrow and arrowhead show full-length L1 (16L1) and short L1 of approximately 15 kDa, respectively. *, unknown nonspecific cellular protein; α-Tub, α-tubulin.

of their transcriptional activity for CLEAR (Coordinated Lysosomal Expression and Regulation) genes (46). In contrast, the loss of FLCN results in the conversion of RagC/D to the inactive, GTP-bound form and decreases the phosphorylation of TFEB and TFE3. These effects lead to the translocation of the transcription factors from the lysosomal

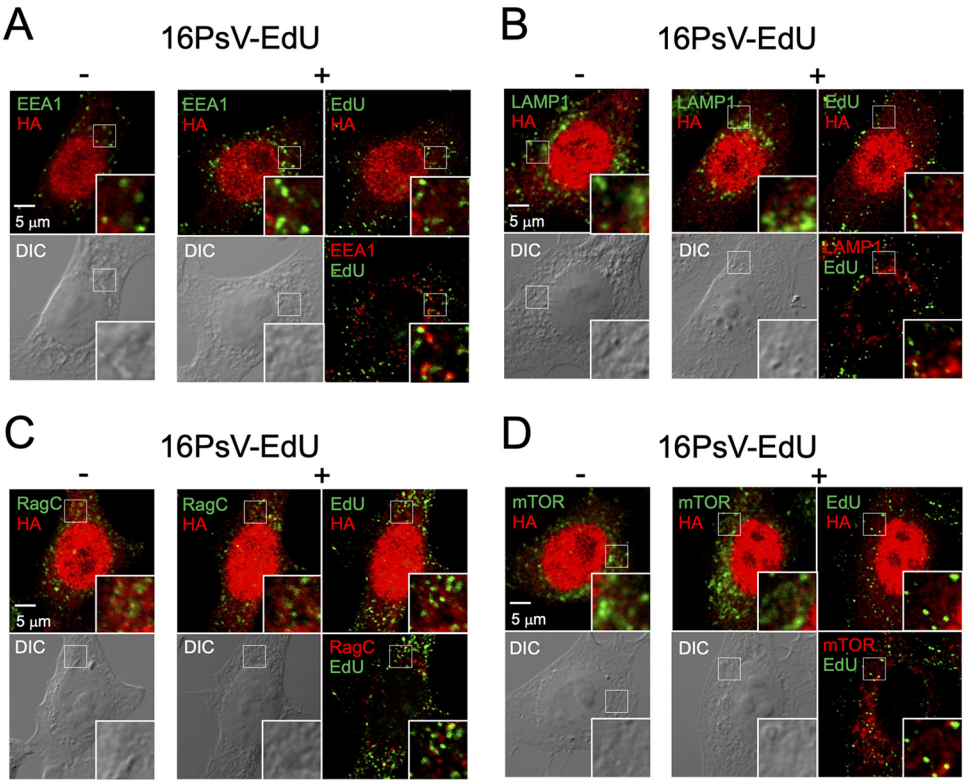

FIG 10 Subcellular localization of FLCN in cells infected with PsVs. ΔFLCN/FLCN-HA cells were incubated with (+) or without (−) 16PsV-EdU at 37°C for 2 h. EdU in the cells was labeled with Alexa Fluor 488 azide by the Click-iT reaction. FLCN-HA (A to D), EEA1 (A), LAMP1 (B), RagC (C), and mTOR (D) were then labeled with their specific antibodies, followed by incubation with anti-mouse or anti-rabbit IgG antibody conjugated with Alexa Fluor 555 or 647. The localizations of FLCN-HA and EdU are shown as red and green signals, respectively. The localizations of EEA1, LAMP1, RagC, and mTOR are shown as green or red signals. DIC, differential interference contrast.

surface to the nucleus, where they induce the transcription of the CLEAR genes (47, 48). Thus, we suggest that FLCN suppresses excessive lysosomal biosynthesis by retaining TFEB and TFE3 on the lysosomal membrane through its GAP activity for RagC (Fig. 11). This process would allow the stable intracellular trafficking of HPV virions. Notably, RagA

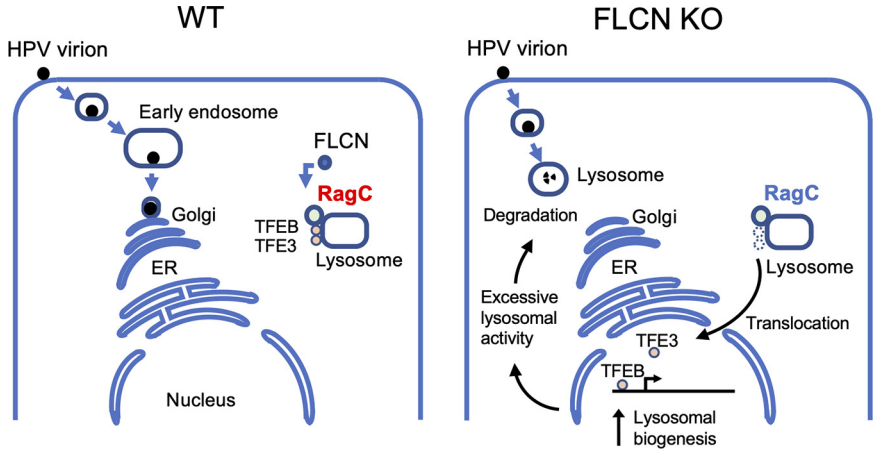

FIG 11 Model of HPV cell entry. In wild-type (WT) cells, HPV virions traffic through the early endosome and reach the Golgi apparatus. FLCN suppresses the induction of lysosomal biogenesis by retaining the transcription factors TFEB and TFE3 on the lysosomal membrane through the activation of RagC (red). In FLCN knockout (KO) cells, TFEB and TFE3 are released from inactive RagC (blue) and translocated into the nucleus, where they induce the transcription of lysosomal genes. This process leads to excessive lysosomal activity and the rapid degradation of virions in the lysosome.

KO exerted a limited effect on PsV infection and L1 degradation compared with RagC KO. This difference may reflect recent evidence implying that active RagA mutants do not fully rescue the phosphorylation and lysosomal recruitment of TFE3 in the absence of FLCN (49), although RagA activation is required for the recruitment of mTORC1 to the lysosomal surface (50).

Our CRISPR-Cas9 KO library screen also revealed sgRNAs for all genes of the γ-secretase complex, which plays crucial roles in the initial stages of HPV infection (17, 20). Although a previous small interfering RNA screen identified components of the γ-secretase complex as being essential for HPV infection, *NCSTN* was not identified in that study (22). The identification of all components of the γ-secretase complex, which promotes the insertion of L2 as a molecular chaperone into the membrane during virus entry (16), suggests that the integrity of the complex is critical in the initial stages of HPV infection.

Our screening results further highlighted the importance of ER-Golgi-related genes in HPV entry. The present findings are consistent with those of previous studies that performed genome-wide screening for RNA interference that inhibited infection of HeLa cells by 16PsVs (22, 25). This evidence suggested that the HPV genome traffics from the Golgi apparatus to the ER following the retrograde transport of virions. Of note, the identified ER-Golgi-related genes also affect HS biosynthesis because the ER-to-Golgi transport system is important for appropriate glycan biosynthesis. Indeed, these genes were previously isolated in genome-wide screens against pathogens that utilize glycans as receptors, including HS in chikungunya virus (51), a glycolipid for the Shiga toxin (52), and N- and O-glycans for the subtilase cytotoxin (53).

TRAPPC12 and TRAPPC13 are required for effective HPV infection. They are components of the TRAPPIII complex (54), which activates Rab1 GTPase and plays essential roles in membrane traffic and autophagy (55). We previously reported that TRAPPC8 (a subunit of TRAPPIII) is essential for the intracellular trafficking of HPV (56). This finding strongly implies that the TRAPPIII complex plays an invaluable role in HPV infection.

Given the protective role of FLCN in HPV infection, patients with FLCN deficiency may be less susceptible to HPV infections. Using PCR, Bradley et al. analyzed clinical specimens obtained from nine patients with BHD syndrome (seven with fibrofolliculoma skin lesions, one with renal cancer, and one with a lung cyst) for the presence of cutaneous and mucosal HPV types. Those investigators did not detect HPV in any of the specimens (57).

In conclusion, in this study, we show that the depletion of FLCN leads to the suppression of HPV infection. Hence, we propose that FLCN prevents the lysosomal degradation of HPV virions as a mechanism for this suppression. These findings have broad implications for research on HPV and basic cell biology. Because the dysregulation of FLCN is responsible for BHD syndrome, the present findings may enhance our understanding of the pathological mechanisms underlying this hereditary disease.

MATERIALS AND METHODS

Cell culture. HeLa-mCAT#8 cells, which express mouse cationic amino acid transporter 1 (a mouse ectotropic retroviral receptor) (58); HaCaT cells (an immortalized human epidermal keratinocyte cell line); Lenti-X 293T cells (TaKaRa Bio, Shiga, Japan); and 293FT cells (Thermo Fisher Scientific, Waltham, MA, USA) were cultured in Dulbecco's modified Eagle's medium (DMEM) (Thermo Fisher Scientific) containing 10% fetal bovine serum (FBS; Nichirei Biosciences, Inc., Tokyo, Japan). Ect1/E6E7 cells (ATCC CRL-2614; American Type Culture Collection, Manassas, VA, USA), an ectocervical cell line immortalized by the expression of HPV16 E6/E7 genes, were maintained in keratinocyte serum-free medium (SFM) (Thermo Fisher Scientific) supplemented with 0.05 mg/mL bovine pituitary extract and 0.1 ng/mL human recombinant epidermal growth factor (Thermo Fisher Scientific).

Plasmids. HPV18 L1 and HPV18 L2 expression plasmids (pCMV-18L1 and pCMV-18L2) were constructed by the insertion of the HPV18 L1 and L2 genes into pCMV-LacZ (TaKaRa Bio), respectively. The HPV18 *L1* and *L2* genes were amplified from peL1fB and peL2bhb, respectively (59), by PCR. The primers used in this experiment were as follows: HPV18 L1 forward primer 5′-TTT TGC GGC CGC GCC ACC ATG GCC CTC TGG AGA CCA TCC GAT AAC, HPV18 L1 reverse primer 5′-TTT TGC GGC CGC TCA TTT GCG TGC CCT CAC TCT GAC, HPV18 L2 forward primer 5′-TTT TGC GGC CGC TCA TTT GCG TGC CCT CAC TCT GAC, and HPV18 L2 reverse primer 5′-TTT TGC GGC CGC TCA AGC GGC GAC GAA CCC GTC GGC. The amplicons were digested by NotI and inserted into pCMV-LacZ at the NotI site following the excision of the β-galactosidase gene from pCMV-LacZ. The bovine papillomavirus E2 gene expression plasmid (pCMS-

BE2-EGFP) was constructed by the insertion of the synthesized bovine papillomavirus E2 gene (Eurofins Genomics, Tokyo, Japan) into pCMS-EGFP (TaKaRa Bio) at the NotI site. To construct the luciferase-expressing reporter plasmid (pCMV-Luc2), DNA encoding firefly luciferase was amplified by PCR, using pGL4.10 (Promega Corp., Madison, WI, USA) as a template. Next, the amplicon was inserted into pCMV-LacZ at the NotI site following the excision of the β-galactosidase gene from pCMV-LacZ. Subsequently, the synthesized simian virus 40 (SV40) origin sequence (Eurofins Genomics) was inserted into the vector.

The human GeCKO v2.0 library in the lentiGuide-Puro plasmid (65,386 sgRNAs in library A and 58,031 sgRNAs in library B) and the lentiCas9-Blast plasmid (two-vector lentiviral GeCKO system) were obtained from Addgene (60). CRISPR plasmids, which are sgRNA expression plasmids containing Cas9 and puromycin resistance genes, were constructed from the pSELECT-CRISPR-Cas9 plasmid (61). The plasmid was cleaved with BsmBI, and a 20-mer guide sequence was ligated into the site. The sgRNA sequences used in this study are described below.

FLCN guide sequence expression plasmids for lentivirus (lentiCRISPRv2 FLCN) were constructed by the insertion of an FLCN sgRNA sequence into lentiCRISPRv2 (Addgene) (60). The FLCN sgRNA sequences were as follows: GGA ATC ATC GAT GAG CTC CA for FLCN-1 and TCA CGC CAT TCC TAC ACC AG for FLCN-2.

FLCN gene expression plasmids for lentivirus (pLVSIN-CMV Neo FLCN-HA) were constructed as follows. The *FLCN* gene was amplified from pF1KE2004 (catalog number FXC28435; Promega Corp.) by PCR. The primers used for FLCN gene amplification were as follows: FLCN forward primer 5′-AGT TCT AGA GCG GCC GCC ACC ATG AAT GCC ATC GTG GCT CTC TG and FLCN reverse primer 5′-CCT CCG CCC GCG GCC GCG TTC CGA GAC TCC GAG GCT GTG GGG. Synthetic oligonucleotides containing an XbaI site, a NotI site, Gly/Ser linkers, HA, and a BamHI site were inserted into pLVSIN-CMV Neo (catalog number 6950; TaKaRa Bio) at the NotI site using the In-Fusion HD cloning kit (TaKaRa Bio) to create pLVSIN-CMV Neo-HA. The synthetic oligonucleotide sequences for pLVSIN-CMV Neo-HA were as follows: sense sequence 5′-CTA GAG CGG CCG CGG GCG GAG GAG GCT CTG GAG GCG GCG GAT CTG GAG GAG GCG GCT CCT ACC CAT ACG ATG TTC CAG ATT ACG CTT GAG and antisense sequence 5′-GAT CCT CAA GCG TAA TCT GGA ACA TCG TAT GGG TAG GAG CCG CCT CCT CCA GAT CCG CCG CCT CCA GAG CCT CCT CCG CCC GCG GCC GCT. The oligonucleotides were annealed and inserted into pLVSIN-CMV Neo at the XbaI and BamHI sites. Next, a human influenza virus HA-tagged FLCN gene expression plasmid (pLVSIN-CMV Neo FLCN-HA) was constructed by the insertion of *FLCN* into pLVSIN-CMV Neo-HA.

Firefly luciferase gene expression plasmids for recombinant lentiviruses (pLVSIN-CMV pur Luc2) and AAV2 (pAAV-CMV Luc2) were constructed as follows. The Luc2 gene was amplified from pGL4.10 (Promega Corp.) by PCR. It was inserted into pLVSIN-CMV pur (TaKaRa Bio) at the NotI site, and into the pAAV-CRE recombinase vector (TaKaRa Bio) at the NotI/SalI sites, following the excision of the CRE recombinase gene from the pAAV-CRE recombinase vector. The cloning reactions were performed using the In-Fusion HD cloning kit (TaKaRa Bio). The primers used for the amplification of the Luc2 gene were as follows: Luc2 for pLVSIN forward primer 5′-AGT TCT AGA GCG GCC GCC ACC ATG GAA GAT GCC AAA AAC ATT AAG, Luc2 for pLVSIN reverse primer 5′-ATT GGA TCC GCG GCC GCT ACA CGG CGA TCT TGC CGC CCT TC, Luc2 for pAAV forward primer 5′-AAG ACC CGG GCG GCC GCC ACC ATG GAA GAT GCC AAA AAC ATT AAG, and Luc2 for pAAV reverse primer 5′-TGC CAC CCG TGT CGA CTA CAC GGC GAT CTT GCC GCC CTT C.

PsVs. HPV18 PsVs containing pCMS-BE2-EGFP (18PsV-BE2) were prepared from 293FT cells transfected with pCMV-18L1, pCMV-18L2, and pCMS-BE2-EGFP, as previously described (59). 18PsV-Luc, an HPV18 L1 and L2 capsid encapsulating pCMV-Luc2, and 16PsV-Luc, an HPV16 L1 and L2 capsid encapsulating pCMV-Luc2, were also prepared as previously described (59). EdU-labeled 18PsVs (18PsV-EdU) and 16PsVs (16PsV-EdU), in which pCMV-Luc2 was labeled with EdU (Thermo Fisher Scientific), were generated in 293FT cells grown in medium containing EdU, as previously described (62). PsV stocks were electrophoresed on a sodium dodecyl sulfate (SDS)-polyacrylamide gel and stained with SYPRO ruby stain (Thermo Fisher Scientific). The L1 capsid protein was quantified using the ChemiDoc imaging system (Bio-Rad, Hercules, CA, USA). After treatment with DNase, the reporter plasmids (vector genomes [vg]) packaged into the PsVs were purified using the QIAamp DNA minikit (Qiagen, Hilden, Germany) and quantified by PCR using the Thunderbird Sybr quantitative PCR (qPCR) mix (Toyobo, Osaka, Japan) on the StepOnePlus real-time PCR system (Thermo Fisher Scientific). The following primers were used in this experiment: pCMS-BE2-EGFP forward primer 5′-GAG CGC ACC ATC TTC AA, pCMS-BE2-EGFP reverse primer 5′-TCC TTG AAG TCG ATG CCC TT, pCMV-Luc2 forward primer 5′-TGA CCG AGA AGG AGA TCG TG, and pCMV-Luc2 reverse primer 5′-GAG AAT CTC GCG GAT CTT GC.

Recombinant lentiviruses. FLCN-sgRNA expression lentivirus (LV FLCN sgRNA), FLCN-HA expression lentivirus (LV FLCN-HA), and firefly luciferase gene expression lentivirus (rLV) were prepared using lentiviral high-titer packaging mix (TaKaRa Bio). Briefly, lentiCRISPR v2 FLCN, pLVSIN-CMV Neo FLCN-HA, or pLVSIN-CMV pur Luc2 was added to the lentiviral high-titer packaging mix. The virus mixtures were introduced into Lenti-X 293T cells (TaKaRa Bio) in 10-cm culture dishes containing the Trans IT-293 reagent (TaKaRa Bio). After 2 days of incubation, the lentivirus-containing supernatants were harvested and concentrated 10-fold using Lenti-X concentrator (TaKaRa Bio). The concentrated viruses were stored at −80°C. The rLV genome (viral genomes per milliliter) titers were measured using the Lenti-X quantitative reverse transcription PCR (qRT-PCR) titration kit (TaKaRa Bio).

Recombinant AAV2. Recombinant AAV2 (rAAV2) expressing the firefly luciferase gene was prepared using the AAVpro helper-free system (TaKaRa Bio). Briefly, pAAV-CMV Luc2 was introduced into 293FT cells (Thermo Fisher Scientific) in the presence of Trans IT-293 reagent (TaKaRa Bio) in 10-cm culture dishes together with the pRC2-mi342 (TaKaRa Bio) and pHelper (TaKaRa Bio) vectors. After 2 days of incubation, rAAV2 was extracted from the cells using an AAV extraction solution (TaKaRa Bio) and stored at −80°C. The rAAV2 genomic titer was measured using the AAVpro titration kit, version 2 (TaKaRa Bio).

Preparation of sgRNA-expressing cell libraries. Four independent sgRNA-expressing cell libraries (A1, A2, B1, and B2) were prepared as previously described (52). Briefly, cell cultures of the HeLa CAS9#W7 cell clone (*Streptococcus pyogenes* Cas9 expressing) were infected at a low multiplicity of infection (approximately 0.2) by four independent lentiviral pools (A1, A2, B1, and B2) from the GeCKO v2.0 library. After 24 h of incubation, the cells were cultured for 3 days with 1 μg/mL puromycin. This was followed by culture in puromycin-free medium for an additional 5 days. These cell libraries were frozen and stored at −80°C until use.

CRISPR screening for 18PsV-BE2 infection. A1, A2, B1, and B2 sgRNA-expressing cells were seeded into 12 culture dishes (150 mm) (2.5×10^6 cells/dish [total of 3×10^7 cells]). After 16 h of incubation, the cells were infected with 18PsV-BE2 at 17.3×10^3 vg/cell (60 μg of L1/dish). The following day, a second 18PsV-BE2 infection was performed at the same concentration. Four days later, the culture medium was replaced. After 3 days of incubation, the cells were split to 2.5×10^6 cells/dish on 12 dishes to equal a total of 3×10^7 cells. Following an additional 3 days of incubation, the culture medium was replaced. After another incubation period of 3 days (i.e., a total of 14 days after the first infection), the cells were collected and frozen at −80°C.

For the uninfected control, 1.5×10^7 sgRNA-expressing cells from each cell library were seeded onto six 150-mm cell culture dishes at 2.5×10^6 cells/dish. After 3 days of incubation, the medium was replaced. Following an additional 3 days of incubation, the cells were split to 2.5×10^6 cells per 150-mm dish on six dishes. After 3 days of incubation, the medium was replaced. After another incubation period of 3 days, the cells were split to a total of 1.5×10^7 cells on six dishes. Finally, after 3 days of incubation, the cells were harvested and frozen at −80°C.

Genomic DNA sequencing. Genomic DNA extracted from frozen cells was purified using the conventional phenol-chloroform method (52). The amplification of genome-integrated sgRNA sequences and the analysis of the sequences using the MiSeq platform (Illumina, San Diego, CA, USA) were performed as previously described (52).

Data processing and analysis. Data processing and analysis were performed as previously described (52, 63). Statistical data for the enriched genes were obtained using the MAGeCK method. In our CRISPR screen, we selected 550 genes from the MAGeCK analysis, which enables the robust identification of essential genome-scale CRISPR-Cas9 KO screens (64); a *P* value of <0.01 was used as the cutoff value (see Data Set S4 in the supplemental material). The results were visualized by a Manhattan plot produced by the Plotly Java Script open-source graphing library (plotly.js version 1.50.0).

Preparation of sgRNA-treated cells. HeLa-mCAT#8 cells were transfected with a CRISPR plasmid and screened with puromycin to remove untransfected cells, as previously described (52). Briefly, HeLa-mCAT#8 cells in 12-well culture dishes were transfected with an empty plasmid or a CRISPR plasmid. The following day, the cells were transferred to six-well culture dishes containing medium with puromycin (5 μg/mL medium). Three days later, the culture medium was replaced with puromycin-free medium. After 3 days of incubation, the CRISPR-treated HeLa cells were used for experiments involving HPV PsV infections or were cloned to isolate single-KO clones. The sgRNA target sequences were as follows: NDST1, 5′-ATG ACG CAC CTG TCC AAC TA; EXT2, 5′-CGA TTA CCC ACA GGT GCT AC; EXTL3, 5′-TGA ACA ACC GAT TCT TAC CC; XYLT2, 5′-TGG TGG ATG GCG GTT CTG AC; HS6ST1, 5′-TCA TGC AGT ACA ATA GCA CG; B4GALT7, 5′-CAG CAG GAT GCC GCC GAC AT; EXT1, 5′-GCC AGT GTT GAA GCT TCT CG; APH1A, 5′-TTA CTT AAG CAG CTT GTA GT; NCSTN, 5′-CTA CAG TGG GTA TTG ACT GA; PSENEN, 5′-TAG ACT CAC AGC CTT TGA TT; PSEN1, 5′-TGG GGT CGT CCA TTA GAT AA; PSEN2, 5′-CAT CAT GAT CAG TGC GCT CA; FLCN, 5′-GGA ATC ATC GAT GAG CTC CA; RRAGC, 5′-CAT TCC ACA ACT GCC GAC CT; RICTOR, 5′-AAA ACT GGG CTT TCA CTA TG; RRAGA, 5′-GGT GTC GCG AGC AAT GTA AT; UNC50, 5′-AGC CCG TAG AGC AGA ATC AG; RER1, 5′-GAC CCA TCG CAC AGC CGT GT; TRAPPC12, 5′-TAG TAC TCG TAA TAA AGA TC; COG4, 5′-CAA CCT CGC CAC CAC AGA GC; TRAPPC13, 5′-ACA TCA TCA ATA CAA CAA TC; SEC31A, 5′-CCT GAA TTG TTA CTG AGC TG; GPR89A, 5′-CCA TAG AAC AGC TCA TCA GC; SEC23IP, 5′-ATG AGC CTG TTC AGC CCC AC; GPR89B, 5′-AAA GAT GAT GAG CTC AAA CA; RAB1B, 5′-TCT TAC TCA CAG CAA ACC GC; RAB1A, 5′-TTA CTG CAA ACC TAA GAA GA; TMEM147, 5′-GTC ATA GAT GCC GCC TTC CC; USO1, 5′-TGT AGT ACT TCT CAT GTC CA; TBC1D5, 5′-TTC CTC AAG ACA AAA GTC AA; SEC23B, 5′-TTG ATT ATC GAG CAA AAC TT; GOSR2, 5′-ATT CAG CCG TCT AGA ACG TC; PSMD12, 5′-TCA CTA CTG CAA CTA AGA TA; FURIN, 5′-TCG GGG ACT ATT ACC ACT TC; PDS5A, 5′-GCT TCT GAA TCA ATG TGC AC; OLFML2B, 5′-CGA ACC GAG ATG AAT AAG CG; SPPL3, 5′-CTT GTT AAA TAC TGG CAC AT; CLMP, 5′-TGG CTG CTC ACC GAT AAT GA; UBE3D, 5′-CTT GTA CCT TCC TCT TGC CG; UNC45B, 5′-GGG CAC TTA CTC TGG CTT GG; and B3GAT3, 5′-GTG TGT GAA GAG GAG GCC AG.

Insertion/deletion analysis. Clones of plasmid-based CRISPR-treated FLCN KO (ΔFLCN), RagA KO (ΔRagA), and RagC KO (ΔRagC) HeLa cells were lysed in lysis buffer for analysis by PCR (TaKaRa Bio). PCR was performed with TKs Gflex DNA polymerase (TaKaRa Bio). The products were subjected to ExoSAP-IT Express PCR product cleanup (Thermo Fisher Scientific), which was followed by DNA sequence analysis on an ABI3730xl genetic analyzer (Applied Biosystems, Waltham, MA, USA). Alternatively, the PCR product was treated with 10× A attachment mix (Toyobo), and pGEM-T Easy vector system I was used to clone the treated PCR products (Promega Corp.). The plasmids were subsequently transformed into *Escherichia coli* and purified for use as the templates for the sequence analysis. The primers used for PCR were as follows: FLCN forward primer 5′-TGT TCA GCC ACA CCT TCT TCA TC, FLCN reverse primer 5′-AGA GAC TAC AAT TCA CAC AGT GC, RagA (RRAGA) forward primer 5′-CCG GCG GGT GAT GCC AAA TAC AG, RagA (RRAGA) reverse primer 5′-TCG CGG CTC TCC ACG TCA AAC AC, RagC (RRAGC) forward primer 5′-TTT GAA GCC TTT AGT AAG GTG G, and RagC (RRAGC) reverse primer 5′-TGC TAT CAA GAA AGG CGT TAT G. The generation of the B3GAT3 KO cell clone was performed as previously described (52). The

primers used for PCR to check for mutations were as follows: B3GAT3 forward primer 5′-CTG GTA CAG AAG GCA GAG CTG and B3GAT3 reverse primer 5′-GCA AAG TAG ACG ACT CCT TGG G.

Reintroduction of FLCN into FLCN KO cells. Stable monoclonal FLCN-reintroduced ΔFLCN cells (ΔFLCN/FLCN-HA) were prepared by transduction with LV FLCN-HA. ΔFLCN cells were transduced with LV FLCN-HA at 100 vg/cell and screened using medium containing 800 μg Geneticin/mL (Thermo Fisher Scientific).

Lentivirus-based FLCN KO cells. FLCN KO HaCaT cells and FLCN KO Ect1/E6E7 cells were prepared by transduction with LV FLCN sgRNA. HaCaT cells (1.5×10^5 cells/well in 12-well culture dishes) and Ect1/E6E7 cells (1.5×10^5 cells/well in 12-well culture dishes) were grown in the appropriate culture medium for each cell type as described above. The following day, the cells were transduced with an LV FLCN sgRNA stock solution (20-fold dilution in each culture medium). After 24 h, the medium was replaced with medium containing 1 μg puromycin/mL. After 3 days of incubation, the cells were transferred to six-well culture dishes containing medium with 1 μg puromycin/mL. After 5 days of incubation, the lentivirus-transduced cells were used for experiments on HPV PsV infections. The culture medium containing puromycin was replaced every 48 h.

PsV infection. HeLa-mCAT#8, CRISPR plasmid-treated HeLa-mCAT#8, ΔFLCN, ΔFLCN/FLCN-HA, ΔRagA, and ΔRagC cells (0.5×10^4 cells/well in 96-well culture dishes); LV FLCN sgRNA-transduced HaCaT cells (0.5×10^4 cells/well in 96-well culture dishes); and LV FLCN sgRNA-transduced Ect1/E6E7 cells (1.0×10^4 cells/well in 96-well culture dishes) were cultured in DMEM containing 10% FBS. The following day, the cells were infected with 18PsV-Luc or 16PsV-Luc at 161 vg/cell (for 18PsV-Luc, 0.004 μg of L1/well; for 16PsV-Luc, 0.01 μg of L1/well) in culture medium. After 2 days of incubation, the luciferase activity in the cells was measured using a luciferase assay system (Promega Corp.) on a Mithras LB940 plate reader (Berthold Technologies, Bad Wildbad, Germany). The activity was normalized to the cell viability, which was estimated using the CellTiter 96 nonradioactive cell proliferation assay (Promega Corp.). The experiments were independently repeated three times.

rLV and rAAV2 infection. ΔFLCN cells and their parent cells (HeLa-mCAT#8 cells) were seeded into 96-well culture dishes (0.5×10^4 cells/well), incubated for 1 day, and subsequently infected with rLV or rAAV2 at 10 vg/cell. After 2 days of incubation, the luciferase activity in the cells was measured and normalized as described above. The experiments were independently repeated three times.

Western blot analysis. Cells grown in a 24-well plate were lysed in SDS sample buffer containing dithiothreitol, and the lysates were denatured at 98°C for 10 min. The proteins in the lysates were separated by SDS-polyacrylamide gel electrophoresis and transferred onto a polyvinylidene difluoride membrane using the iBlot gel transfer system (Thermo Fisher Scientific). The membrane was incubated with 10% skimmed milk in phosphate-buffered saline (PBS) at room temperature (RT) for 1 h; washed with 0.5% Tween 20 in PBS (PBST); and incubated with rabbit monoclonal anti-FLCN antibody (clone EPNCIR147; Abcam, Cambridge, UK), rabbit monoclonal anti-RagA antibody (clone D8B5; Cell Signaling Technology, Danvers, MA, USA), rabbit monoclonal anti-RagC antibody (clone D8H5; Cell Signaling Technology), or mouse monoclonal anti-α-tubulin antibody (catalog number T-9026; Sigma-Aldrich, St. Louis, MO, USA) at 4°C overnight. Subsequently, the membrane was washed in PBST and incubated with goat anti-rabbit or anti-mouse immunoglobulin G (IgG) conjugated with horseradish peroxidase (Santa Cruz Biotechnology, Santa Cruz, CA, USA) at RT for 1 h. Immunoreactive proteins were detected using the Amersham ECL Prime Western blotting detection reagent (GE Healthcare, Chicago, IL, USA) on a ChemiDoc XRS+ system (Bio-Rad).

Immunofluorescence microscopy. For the analysis of cell surface binding, HeLa-mCAT#8, ΔFLCN, ΔFLCN/FLCN-HA, and B3CAT3 KO cells (1×10^4 cells/well in an eight-well chamber slide) were incubated with 18PsV-Luc (0.1 μg L1/well) in culture medium at 4°C for 1 h. The cells were washed in PBS, fixed with 4% paraformaldehyde in PBS, and blocked with 5% normal goat serum (NGS) in PBS at RT for 30 min. Thereafter, they were incubated with mouse monoclonal anti-HPV18 L1 antibody (clone H18.J4) (a kind gift from Neil Christensen, Pennsylvania State University, State College, PA, USA) or mouse IgM κ-chain anti-HS antibody (clone F58-10E4; Amsbio, Abingdon, UK) diluted 1:100 in 2.5% NGS in PBS at RT for 1 h. This was followed by incubation with Alexa Fluor 555 or 488 dye-conjugated goat anti-mouse IgG(H+L) (Thermo Fisher Scientific) diluted 1:800 in 2.5% NGS in PBS at RT for 45 min.

For the analysis of subcellular localization, HeLa-mCAT#8, ΔFLCN, and ΔFLCN/FLCN-HA cells (1×10^4 cells/well in an eight-well chamber slide) were incubated with 18PsV-EdU or 16PsV-EdU (0.2 μg of L1/well) at 37°C for 2 or 8 h. After washing in PBS, the cells were fixed with 4% paraformaldehyde in PBS and permeabilized with 0.5% Triton X-100 in PBS. Subsequently, the cells were washed three times with 3% bovine serum albumin in PBS, and EdU was labeled with Alexa Fluor 488 azide through a Click-iT reaction (Thermo Fisher Scientific). The cells were incubated with 5% NGS in PBS at RT for 30 min, followed by incubation with rabbit monoclonal anti-EEA1 antibody (clone C45B10; Cell Signaling Technology), mouse monoclonal anti-GM130 antibody (catalog number 610822; BD Biosciences Pharmingen, San Diego, CA, USA), mouse monoclonal anti-HA antibody (clone 16B12; BioLegend, San Diego, CA, USA), rabbit anti-LAMP1 antibody (clone D2D11; Cell Signaling Technology), rabbit monoclonal anti-RagC antibody (clone D8H5; Cell Signaling Technology), or rabbit monoclonal anti-mTOR antibody (clone 7C10; Cell Signaling Technology) diluted 1:100 in 2.5% NGS in PBS at RT for 1 h. After washing, the cells were incubated with Alexa Fluor 546-conjugated goat anti-rabbit IgG (H+L) (Thermo Fisher Scientific), Alexa Fluor 555-conjugated goat anti-mouse IgG(H+L) (Thermo Fisher Scientific), or Alexa Fluor 647-conjugated goat anti-rabbit IgG(H+L) (Thermo Fisher Scientific) diluted 1:800 in 2.5% NGS in PBS at RT for 45 min.

All cells were mounted using ProLong gold antifade mountant with DAPI (4′,6-diamidino-2-phenylindole) (Thermo Fisher Scientific). Finally, fluorescence images were captured using a FluoView FV1000 confocal microscope (Olympus, Tokyo, Japan).

To examine the effects of lysosome protease inhibitors on the subcellular localization of PsVs, HeLa-mCAT#8 and ΔFLCN cells (1×10^4 cells/well in an eight-well chamber slide) were incubated with 16PsV-

EdU (0.2 μg of L1/well) at 37°C for 8 h in the presence or absence of 87.6 μM E64d (Peptide Institute, Inc., Osaka, Japan) and 43.7 μM pepstatin A (Peptide Institute, Inc.). HPV16 L1 was labeled by mouse anti-33L1-7 antibody (a kind gift from Martin Sapp), which recognizes an internal epitope of the L1 capsid (65), and Alexa Fluor 555-conjugated goat anti-mouse IgG(H+L) (Thermo Fisher Scientific). RagC (a lysosome marker) was labeled by anti-RagC antibody (clone D8H5; Cell Signaling Technology) and Alexa Fluor 647-conjugated goat anti-mouse IgG(H+L) (Thermo Fisher Scientific). Fluorescence images were taken as described above.

For virion binding, the fluorescence intensity was quantified in four different fields (approximately 10 cells/field) using FluoView FV1000 software (Olympus) and averaged. The experiment was independently performed three times. The colocalization signals in the merged images from at least 30 cells were quantified using FluoView FV1000 software and evaluated using Pearson's correlation coefficient.

Fluorescence-activated cell sorting analysis. Cells were trypsinized and washed with culture medium and wash buffer (1% bovine serum albumin) in PBS at 4°C. Next, the cells were incubated with mouse anti-HS monoclonal antibody (clone F58-10E4; Amsbio) at a 200-fold dilution or control mouse IgM (BD Biosciences, Franklin Lakes, NJ, USA) for 40 min on ice. After washing with wash buffer, the cells were incubated with Alexa Fluor 488-conjugated anti-mouse IgG (heavy plus light chains, which can recognize IgM) for 30 min on ice. After washing with wash buffer, the cells were analyzed using a FACSCalibur flow cytometer (BD Biosciences).

Virion internalization analysis. HeLa-mCAT#8, ΔFLCN, ΔFLCN/FLCN-HA, ΔRagA, and ΔRagC cells (2.5×10^4 cells/well in a 24-well plate) were incubated with 16PsV-Luc (0.5 μg of L1/well) for 1 h at 4°C. The cells were washed with PBS and detached from the cell culture dishes using EDTA (time zero, without trypsin) or trypsin-EDTA (time zero, with trypsin) or washed with medium and incubated at 37°C for 1, 2, 4, or 8 h. Alternatively, the cells were washed with medium and incubated with or without 20 nM bafilomycin A1 (BafA1) (catalog number B1793; Sigma-Aldrich) or 87.6 μM E64d and 43.7 μM pepstatin A at 37°C for 1, 4, or 8 h. The cells were detached using trypsin-EDTA and lysed in SDS sample buffer. 16PsV-Luc in the lysate was analyzed by Western blotting using a mouse monoclonal anti-HPV16 L1 antibody (catalog number 554171; BD Biosciences Pharmingen) as described above. The band intensity was quantified using ChemiDoc XRS+ system software. The experiments were independently performed three times.

Cellular internalization analysis. The internalization assay for Tf was performed as previously described (56). Briefly, HeLa mCAT8 (control) or ΔFLCN cells were incubated with Tf conjugated with Alexa Fluor 568 (Thermo Fisher Scientific) at 4°C for 1 h and cultured at 37°C for 15 min. The cells were washed with ice-cold PBS, and cell surface-bound Tf was removed by treatment with DMEM containing 25 mM sodium acetate (pH 2.0) on ice for 2 min. The cells were then fixed, permeabilized, and incubated with rabbit monoclonal anti-LAMP1 antibody (clone D2D11; Cell Signaling Technology) and goat anti-rabbit IgG(H+L) conjugated with Alexa Fluor 488 (Thermo Fisher Scientific). The fluorescence in three different fields (approximately 10 cells per field) was quantified using FluoView FV1000 software and averaged. The data are shown as the means ± standard deviations from three independent experiments. Statistical analysis was performed using Student's *t* test. Colocalization signals between Tf and LAMP1 in the merged images obtained from at least 30 cells were quantified using FluoView FV1000 software, and Pearson's correlation coefficient was calculated.

For the analysis of endocytic EGFR, HeLa mCAT8 (control) or ΔFLCN cells were cultured with or without BafA1 at 37°C for 1 h. The cells were detached from the plates with trypsin-EDTA, and the cell extracts were analyzed by Western blotting with rabbit monoclonal anti-EGFR antibody (clone D38B1; Cell Signaling Technology). The band intensity of EGFR was quantified using the ChemiDoc XRS+ system and normalized to that of α-tubulin. Degradation levels were quantified from the band intensity of EGFR with BafA1 versus EGFR without BafA1. The data are shown as the means ± standard deviations from three independent experiments. Statistical analysis was performed using Student's *t* test.

SUPPLEMENTAL MATERIAL

Supplemental material is available online only.

SUPPLEMENTAL FILE 1, XLSX file, 7.1 MB.

SUPPLEMENTAL FILE 2, XLSX file, 6.4 MB.

SUPPLEMENTAL FILE 3, XLSX file, 0.04 MB.

SUPPLEMENTAL FILE 4, XLSX file, 0.05 MB.

ACKNOWLEDGMENTS

We thank Neil Christensen and Martin Sapp for providing the anti-HPV18 L1 (clone H18.J4) and anti-33L1-7 antibodies, respectively.

This work was supported by grants-in-aid for scientific research (C) from the Japan Society for the Promotion of Science (grant number JP18K07154).

REFERENCES

1. Doorbar J. 2018. Host control of human papillomavirus infection and disease. Best Pract Res Clin Obstet Gynaecol 47:27–41. https://doi.org/10.1016/j.bpobgyn.2017.08.001.
2. Van Doorslaer K, Li Z, Xirasagar S, Maes P, Kaminsky D, Liou D, Sun Q, Kaur R, Huyen Y, McBride AA. 2017. The Papillomavirus Episteme: a major update to the papillomavirus sequence database. Nucleic Acids Res 45:D499–D506. https://doi.org/10.1093/nar/gkw879.
3. Conway MJ, Meyers C. 2009. Replication and assembly of human papillomaviruses. J Dent Res 88:307–317. https://doi.org/10.1177/0022034509333446.

4. zur Hausen H. 2002. Papillomaviruses and cancer: from basic studies to clinical application. Nat Rev Cancer 2:342–350. https://doi.org/10.1038/nrc798.
5. Buck CB, Pastrana DV, Lowy DR, Schiller JT. 2004. Efficient intracellular assembly of papillomaviral vectors. J Virol 78:751–757. https://doi.org/10.1128/jvi.78.2.751-757.2004.
6. Joyce JG, Tung JS, Przysiecki CT, Cook JC, Lehman ED, Sands JA, Jansen KU, Keller PM. 1999. The L1 major capsid protein of human papillomavirus type 11 recombinant virus-like particles interacts with heparin and cell-surface glycosaminoglycans on human keratinocytes. J Biol Chem 274:5810–5822. https://doi.org/10.1074/jbc.274.9.5810.
7. Giroglou T, Florin L, Schafer F, Streeck RE, Sapp M. 2001. Human papillomavirus infection requires cell surface heparan sulfate. J Virol 75:1565–1570. https://doi.org/10.1128/JVI.75.3.1565-1570.2001.
8. Surviladze Z, Sterkand RT, Ozbun MA. 2015. Interaction of human papillomavirus type 16 particles with heparan sulfate and syndecan-1 molecules in the keratinocyte extracellular matrix plays an active role in infection. J Gen Virol 96:2232–2241. https://doi.org/10.1099/vir.0.000147.
9. Guan J, Bywaters SM, Brendle SA, Ashley RE, Makhov AM, Conway JF, Christensen ND, Hafenstein S. 2017. Cryoelectron microscopy maps of human papillomavirus 16 reveal L2 densities and heparin binding site. Structure 25:253–263. https://doi.org/10.1016/j.str.2016.12.001.
10. Selinka HC, Giroglou T, Nowak T, Christensen ND, Sapp M. 2003. Further evidence that papillomavirus capsids exist in two distinct conformations. J Virol 77:12961–12967. https://doi.org/10.1128/jvi.77.24.12961-12967.2003.
11. Selinka HC, Florin L, Patel HD, Freitag K, Schmidtke M, Makarov VA, Sapp M. 2007. Inhibition of transfer to secondary receptors by heparan sulfate-binding drug or antibody induces noninfectious uptake of human papillomavirus. J Virol 81:10970–10980. https://doi.org/10.1128/JVI.00998-07.
12. Cerqueira C, Liu Y, Kuhling L, Chai W, Hafezi W, van Kuppevelt TH, Kuhn JE, Feizi T, Schelhaas M. 2013. Heparin increases the infectivity of human papillomavirus type 16 independent of cell surface proteoglycans and induces L1 epitope exposure. Cell Microbiol 15:1818–1836. https://doi.org/10.1111/cmi.12150.
13. Cerqueira C, Samperio Ventayol P, Vogeley C, Schelhaas M. 2015. Kallikrein-8 proteolytically processes human papillomaviruses in the extracellular space to facilitate entry into host cells. J Virol 89:7038–7052. https://doi.org/10.1128/JVI.00234-15.
14. Richards RM, Lowy DR, Schiller JT, Day PM. 2006. Cleavage of the papillomavirus minor capsid protein, L2, at a furin consensus site is necessary for infection. Proc Natl Acad Sci U S A 103:1522–1527. https://doi.org/10.1073/pnas.0508815103.
15. Schelhaas M, Shah B, Holzer M, Blattmann P, Kuhling L, Day PM, Schiller JT, Helenius A. 2012. Entry of human papillomavirus type 16 by actin-dependent, clathrin- and lipid raft-independent endocytosis. PLoS Pathog 8:e1002657. https://doi.org/10.1371/journal.ppat.1002657.
16. Inoue T, Zhang P, Zhang W, Goodner-Bingham K, Dupzyk A, DiMaio D, Tsai B. 2018. γ-Secretase promotes membrane insertion of the human papillomavirus L2 capsid protein during virus infection. J Cell Biol 217:3545–3559. https://doi.org/10.1083/jcb.201804171.
17. Huang H-S, Buck CB, Lambert PF. 2010. Inhibition of gamma secretase blocks HPV infection. Virology 407:391–396. https://doi.org/10.1016/j.virol.2010.09.002.
18. Zhang W, Kazakov T, Popa A, DiMaio D. 2014. Vesicular trafficking of incoming human papillomavirus 16 to the Golgi apparatus and endoplasmic reticulum requires γ-secretase activity. mBio 5:e01777-14. https://doi.org/10.1128/mBio.01777-14.
19. Harwood MC, Dupzyk AJ, Inoue T, DiMaio D, Tsai B. 2020. p120 catenin recruits HPV to gamma-secretase to promote virus infection. PLoS Pathog 16:e1008946. https://doi.org/10.1371/journal.ppat.1008946.
20. Karanam B, Peng S, Li T, Buck C, Day PM, Roden RB. 2010. Papillomavirus infection requires gamma secretase. J Virol 84:10661–10670. https://doi.org/10.1128/JVI.01081-10.
21. Bergant Marusic M, Ozbun MA, Campos SK, Myers MP, Banks L. 2012. Human papillomavirus L2 facilitates viral escape from late endosomes via sorting nexin 17. Traffic 13:455–467. https://doi.org/10.1111/j.1600-0854.2011.01320.x.
22. Lipovsky A, Popa A, Pimienta G, Wyler M, Bhan A, Kuruvilla L, Guie MA, Poffenberger AC, Nelson CD, Atwood WJ, DiMaio D. 2013. Genome-wide siRNA screen identifies the retromer as a cellular entry factor for human papillomavirus. Proc Natl Acad Sci U S A 110:7452–7457. https://doi.org/10.1073/pnas.1302164110.
23. Xie J, Heim EN, Crite M, DiMaio D. 2020. TBC1D5-catalyzed cycling of Rab7 is required for retromer-mediated human papillomavirus trafficking during virus entry. Cell Rep 31:107750. https://doi.org/10.1016/j.celrep.2020.107750.
24. Pyeon D, Pearce SM, Lank SM, Ahlquist P, Lambert PF. 2009. Establishment of human papillomavirus infection requires cell cycle progression. PLoS Pathog 5:e1000318. https://doi.org/10.1371/journal.ppat.1000318.
25. Aydin I, Weber S, Snijder B, Samperio Ventayol P, Kuhbacher A, Becker M, Day PM, Schiller JT, Kann M, Pelkmans L, Helenius A, Schelhaas M. 2014. Large scale RNAi reveals the requirement of nuclear envelope breakdown for nuclear import of human papillomaviruses. PLoS Pathog 10:e1004162. https://doi.org/10.1371/journal.ppat.1004162.
26. DiGiuseppe S, Luszczek W, Keiffer TR, Bienkowska-Haba M, Guion LG, Sapp MJ. 2016. Incoming human papillomavirus type 16 genome resides in a vesicular compartment throughout mitosis. Proc Natl Acad Sci U S A 113:6289–6294. https://doi.org/10.1073/pnas.1600638113.
27. Calton CM, Bronnimann MP, Manson AR, Li S, Chapman JA, Suarez-Berumen M, Williamson TR, Molugu SK, Bernal RA, Campos SK. 2017. Translocation of the papillomavirus L2/vDNA complex across the limiting membrane requires the onset of mitosis. PLoS Pathog 13:e1006200. https://doi.org/10.1371/journal.ppat.1006200.
28. Lai K-Y, Rizzato M, Aydin I, Villalonga-Planells R, Drexler HCA, Schelhaas M. 2021. A Ran-binding protein facilitates nuclear import of human papillomavirus type 16. PLoS Pathog 17:e1009580. https://doi.org/10.1371/journal.ppat.1009580.
29. Aydin I, Villalonga-Planells R, Greune L, Bronnimann MP, Calton CM, Becker M, Lai K-Y, Campos SK, Schmidt MA, Schelhaas M. 2017. A central region in the minor capsid protein of papillomaviruses facilitates viral genome tethering and membrane penetration for mitotic nuclear entry. PLoS Pathog 13:e1006308. https://doi.org/10.1371/journal.ppat.1006308.
30. Ramirez Reyes JMJ, Cuesta R, Pause A. 2021. Folliculin: a regulator of transcription through AMPK and mTOR signaling pathways. Front Cell Dev Biol 9:667311. https://doi.org/10.3389/fcell.2021.667311.
31. de Martin Garrido N, Aylett CHS. 2020. Nutrient signaling and lysosome positioning crosstalk through a multifunctional protein, folliculin. Front Cell Dev Biol 8:108. https://doi.org/10.3389/fcell.2020.00108.
32. Tsun Z-Y, Bar-Peled L, Chantranupong L, Zoncu R, Wang T, Kim C, Spooner E, Sabatini DM. 2013. The folliculin tumor suppressor is a GAP for the RagC/D GTPases that signal amino acid levels to mTORC1. Mol Cell 52:495–505. https://doi.org/10.1016/j.molcel.2013.09.016.
33. Lawrence RE, Fromm SA, Fu Y, Yokom AL, Kim DJ, Thelen AM, Young LN, Lim C-Y, Samelson AJ, Hurley JH, Zoncu R. 2019. Structural mechanism of a Rag GTPase activation checkpoint by the lysosomal folliculin complex. Science 366:971–977. https://doi.org/10.1126/science.aax0364.
34. Petit CS, Roczniak-Ferguson A, Ferguson SM. 2013. Recruitment of folliculin to lysosomes supports the amino acid-dependent activation of Rag GTPases. J Cell Biol 202:1107–1122. https://doi.org/10.1083/jcb.201307084.
35. Laviolette LA, Mermoud J, Calvo IA, Olson N, Boukhali M, Steinlein OK, Roider E, Sattler EC, Huang D, Teh BT, Motamedi M, Haas W, Iliopoulos O. 2017. Negative regulation of EGFR signalling by the human folliculin tumour suppressor protein. Nat Commun 8:15866. https://doi.org/10.1038/ncomms15866.
36. Nookala RK, Langemeyer L, Pacitto A, Ochoa-Montano B, Donaldson JC, Blaszczyk BK, Chirgadze DY, Barr FA, Bazan JF, Blundell TL. 2012. Crystal structure of folliculin reveals a hidDENN function in genetically inherited renal cancer. Open Biol 2:120071. https://doi.org/10.1098/rsob.120071.
37. Zheng J, Duan B, Sun S, Cui J, Du J, Zhang Y. 2017. Folliculin interacts with Rab35 to regulate EGF-induced EGFR degradation. Front Pharmacol 8:688. https://doi.org/10.3389/fphar.2017.00688.
38. Zhao L, Ji X, Zhang X, Li L, Jin Y, Liu W. 2018. FLCN is a novel Rab11A-interacting protein that is involved in the Rab11A-mediated recycling transport. J Cell Sci 131:jcs218792. https://doi.org/10.1242/jcs.218792.
39. Goodwin EC, DiMaio D. 2000. Repression of human papillomavirus oncogenes in HeLa cervical carcinoma cells causes the orderly reactivation of dormant tumor suppressor pathways. Proc Natl Acad Sci U S A 97:12513–12518. https://doi.org/10.1073/pnas.97.23.12513.
40. Goodwin EC, Yang E, Lee CJ, Lee HW, DiMaio D, Hwang ES. 2000. Rapid induction of senescence in human cervical carcinoma cells. Proc Natl Acad Sci U S A 97:10978–10983. https://doi.org/10.1073/pnas.97.20.10978.
41. Surviladze Z, Dziduszko A, Ozbun MA. 2012. Essential roles for soluble virion-associated heparan sulfonated proteoglycans and growth factors in human papillomavirus infections. PLoS Pathog 8:e1002519. https://doi.org/10.1371/journal.ppat.1002519.
42. Trofimenko E, Homma Y, Fukuda M, Widmann C. 2021. The endocytic pathway taken by cationic substances requires Rab14 but not Rab5 and Rab7. Cell Rep 37:109945. https://doi.org/10.1016/j.celrep.2021.109945.

43. Tomas A, Futter CE, Eden ER. 2014. EGF receptor trafficking: consequences for signaling and cancer. Trends Cell Biol 24:26–34. https://doi.org/10.1016/j.tcb.2013.11.002.
44. Sancak Y, Peterson TR, Shaul YD, Lindquist RA, Thoreen CC, Bar-Peled L, Sabatini DM. 2008. The Rag GTPases bind raptor and mediate amino acid signaling to mTORC1. Science 320:1496–1501. https://doi.org/10.1126/science.1157535.
45. Saxton RA, Sabatini DM. 2017. mTOR signaling in growth, metabolism, and disease. Cell 168:960–976. https://doi.org/10.1016/j.cell.2017.02.004.
46. Puertollano R, Ferguson SM, Brugarolas J, Ballabio A. 2018. The complex relationship between TFEB transcription factor phosphorylation and subcellular localization. EMBO J 37:e98804. https://doi.org/10.15252/embj.201798804.
47. Sardiello M, Palmieri M, di Ronza A, Medina DL, Valenza M, Gennarino VA, Di Malta C, Donaudy F, Embrione V, Polishchuk RS, Banfi S, Parenti G, Cattaneo E, Ballabio A. 2009. A gene network regulating lysosomal biogenesis and function. Science 325:473–477. https://doi.org/10.1126/science.1174447.
48. Napolitano G, Di Malta C, Esposito A, de Araujo MEG, Pece S, Bertalot G, Matarese M, Benedetti V, Zampelli A, Stasyk T, Siciliano D, Venuta A, Cesana M, Vilardo C, Nusco E, Monfregola J, Calcagni A, Di Fiore PP, Huber LA, Ballabio A. 2020. A substrate-specific mTORC1 pathway underlies Birt-Hogg-Dube syndrome. Nature 585:597–602. https://doi.org/10.1038/s41586-020-2444-0.
49. Li K, Wada S, Gosis BS, Thorsheim C, Loose P, Arany Z. 2022. Folliculin promotes substrate-selective mTORC1 activity by activating RagC to recruit TFE3. PLoS Biol 20:e3001594. https://doi.org/10.1371/journal.pbio.3001594.
50. Rogala KB, Gu X, Kedir JF, Abu-Remaileh M, Bianchi LF, Bottino AMS, Dueholm R, Niehaus A, Overwijn D, Fils A-CP, Zhou SX, Leary D, Laqtom NN, Brignole EJ, Sabatini DM. 2019. Structural basis for the docking of mTORC1 on the lysosomal surface. Science 366:468–475. https://doi.org/10.1126/science.aay0166.
51. Tanaka A, Tumkosit U, Nakamura S, Motooka D, Kishishita N, Priengprom T, Sa-Ngasang A, Kinoshita T, Takeda N, Maeda Y. 2017. Genome-wide screening uncovers the significance of N-sulfation of heparan sulfate as a host cell factor for chikungunya virus infection. J Virol 91:e00432-17. https://doi.org/10.1128/JVI.00432-17.
52. Yamaji T, Sekizuka T, Tachida Y, Sakuma C, Morimoto K, Kuroda M, Hanada K. 2019. A CRISPR screen identifies LAPTM4A and TM9SF proteins as glycolipid-regulating factors. iScience 11:409–424. https://doi.org/10.1016/j.isci.2018.12.039.
53. Yamaji T, Hanamatsu H, Sekizuka T, Kuroda M, Iwasaki N, Ohnishi M, Furukawa J-I, Yahiro K, Hanada K. 2019. A CRISPR screen using subtilase cytotoxin identifies SLC39A9 as a glycan-regulating factor. iScience 15:407–420. https://doi.org/10.1016/j.isci.2019.05.005.
54. Galindo A, Planelles-Herrero VJ, Degliesposti G, Munro S. 2021. Cryo-EM structure of metazoan TRAPPIII, the multi-subunit complex that activates the GTPase Rab1. EMBO J 40:e107608. https://doi.org/10.15252/embj.2020107608.
55. Barrowman J, Bhandari D, Reinisch K, Ferro-Novick S. 2010. TRAPP complexes in membrane traffic: convergence through a common Rab. Nat Rev Mol Cell Biol 11:759–763. https://doi.org/10.1038/nrm2999.
56. Ishii Y, Nakahara T, Kataoka M, Kusumoto-Matsuo R, Mori S, Takeuchi T, Kukimoto I. 2013. Identification of TRAPPC8 as a host factor required for human papillomavirus cell entry. PLoS One 8:e80297. https://doi.org/10.1371/journal.pone.0080297.
57. Bradley M, Nordfors C, Vlastos A, Ferrara G, Ramqvist T, Dalianis T. 2014. No association between Birt-Hogg-Dube syndrome skin fibrofolliculomas and the first 10 described human polyomaviruses or human papillomaviruses. Virology 468–470:244–247. https://doi.org/10.1016/j.virol.2014.08.011.
58. Yamaji T, Nishikawa K, Hanada K. 2010. Transmembrane BAX inhibitor motif containing (TMBIM) family proteins perturbs a trans-Golgi network enzyme, Gb3 synthase, and reduces Gb3 biosynthesis. J Biol Chem 285:35505–35518. https://doi.org/10.1074/jbc.M110.154229.
59. Kondo K, Ishii Y, Ochi H, Matsumoto T, Yoshikawa H, Kanda T. 2007. Neutralization of HPV16, 18, 31, and 58 pseudovirions with antisera induced by immunizing rabbits with synthetic peptides representing segments of the HPV16 minor capsid protein L2 surface region. Virology 358:266–272. https://doi.org/10.1016/j.virol.2006.08.037.
60. Sanjana NE, Shalem O, Zhang F. 2014. Improved vectors and genome-wide libraries for CRISPR screening. Nat Methods 11:783–784. https://doi.org/10.1038/nmeth.3047.
61. Ogawa M, Matsuda R, Takada N, Tomokiyo M, Yamamoto S, Shizukuishi S, Yamaji T, Yoshikawa Y, Yoshida M, Tanida I, Koike M, Murai M, Morita H, Takeyama H, Ryo A, Guan J-L, Yamamoto M, Inoue J-I, Yanagawa T, Fukuda M, Kawabe H, Ohnishi M. 2018. Molecular mechanisms of Streptococcus pneumoniae-targeted autophagy via pneumolysin, Golgi-resident Rab41, and Nedd4-1-mediated K63-linked ubiquitination. Cell Microbiol 20:e12846. https://doi.org/10.1111/cmi.12846.
62. Ishii Y, Tanaka K, Kondo K, Takeuchi T, Mori S, Kanda T. 2010. Inhibition of nuclear entry of HPV16 pseudovirus-packaged DNA by an anti-HPV16 L2 neutralizing antibody. Virology 406:181–188. https://doi.org/10.1016/j.virol.2010.07.019.
63. Sakuma C, Sekizuka T, Kuroda M, Hanada K, Yamaji T. 2021. Identification of SYS1 as a host factor required for Shiga toxin-mediated cytotoxicity in Vero cells. Int J Mol Sci 22:4936. https://doi.org/10.3390/ijms22094936.
64. Li W, Xu H, Xiao T, Cong L, Love MI, Zhang F, Irizarry RA, Liu JS, Brown M, Liu XS. 2014. MAGeCK enables robust identification of essential genes from genome-scale CRISPR/Cas9 knockout screens. Genome Biol 15:554. https://doi.org/10.1186/s13059-014-0554-4.
65. Sapp M, Kraus U, Volpers C, Snijders PJ, Walboomers JM, Streeck RE. 1994. Analysis of type-restricted and cross-reactive epitopes on virus-like particles of human papillomavirus type 33 and in infected tissues using monoclonal antibodies to the major capsid protein. J Gen Virol 75(Part 12):3375–3383. https://doi.org/10.1099/0022-1317-75-12-3375.